Transition between dead and turbulent zone in protoplanetary disks: why and how it is relevant for planet formation.

Fulvia Pucci

National Institutes of Natural Sciences, Minato City, Tokyo Japan
NAOJ, Japan
Princeton University
LASP, University of Colorado Boulder

K. Tomida, J. Stone, S. Takasao, S. Okamura

Spere, VLT

T-Tauri
10^7years old
M < 3M$_\odot$

FGKM

Up tp 100AU

ALMA

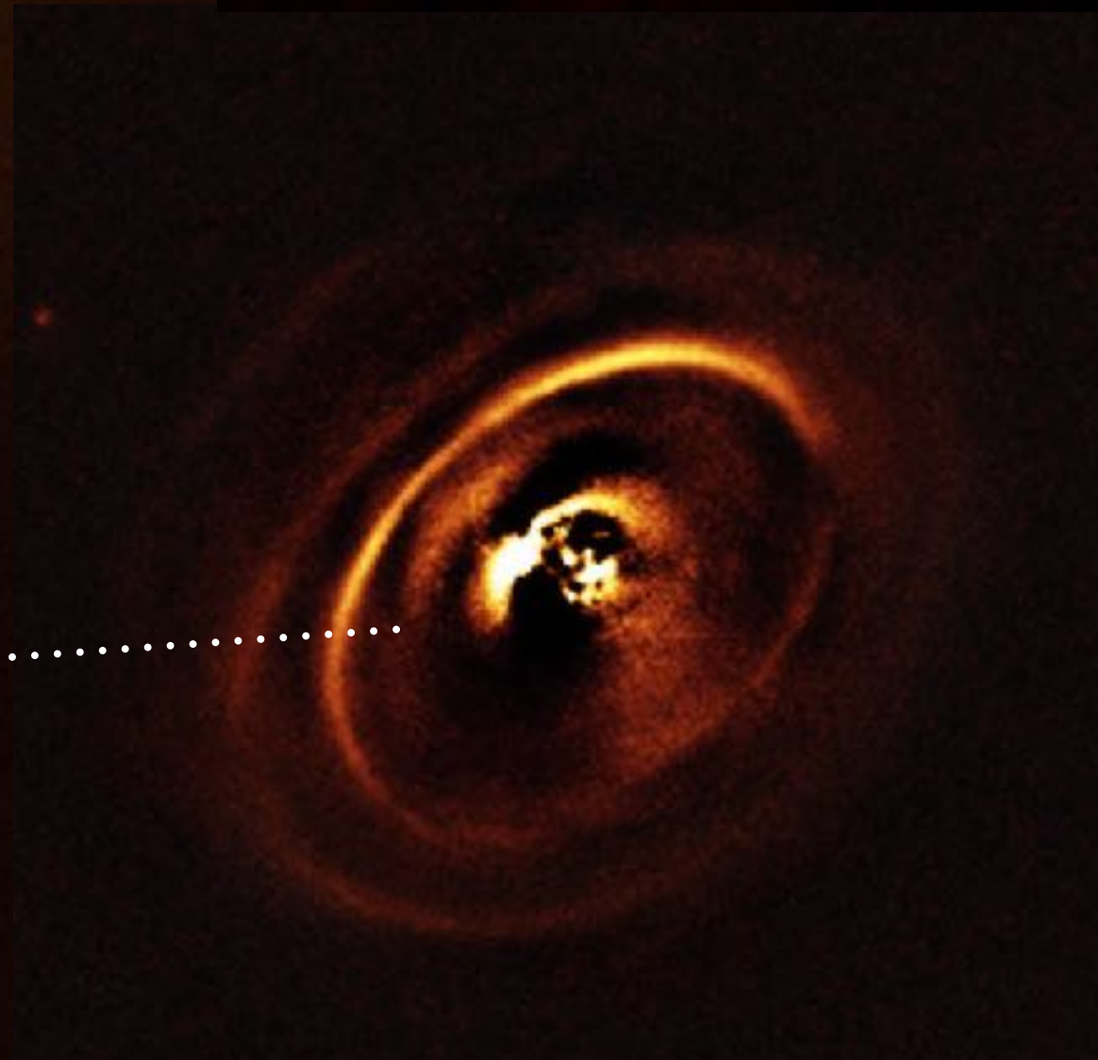

600 ly

What kind of objects are we dealing with?

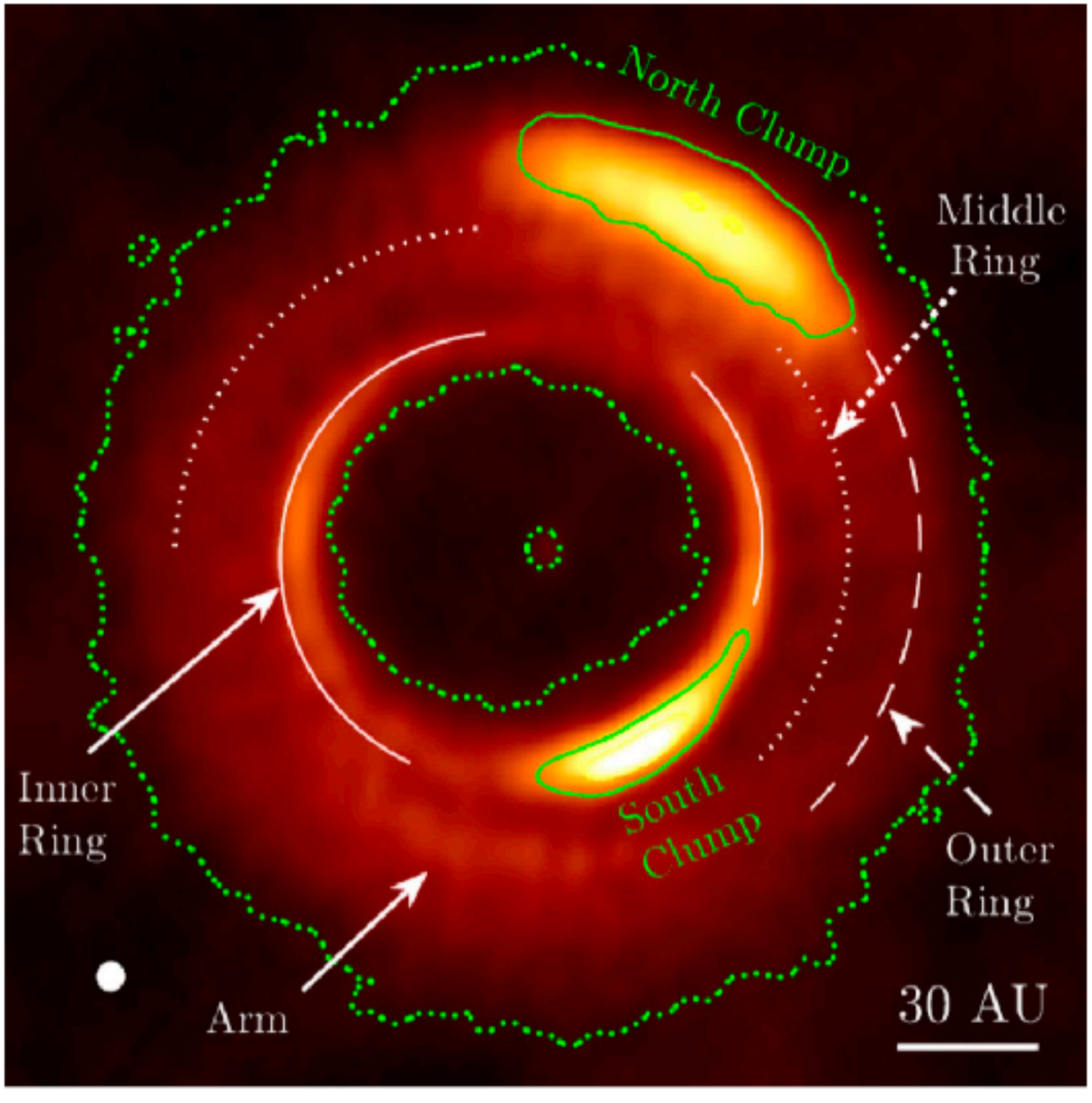

- Plasma and dust accretion
- Experimental study of linear instability (e.g. Richard and Zahn 1999).
- Linear instability mechanisms are not efficient nor reproduce the observed astrophysical time scales. (Ji et al. 2006)
- Linear instability of a stratified flow causing turbulence (e.g. Klahr and Bodenheimer 2003, Urpin 2003).
- The latter mechanism present or inefficient (e.g. Arlt and Urpin 2004 …).

Protoplanetary disk structure

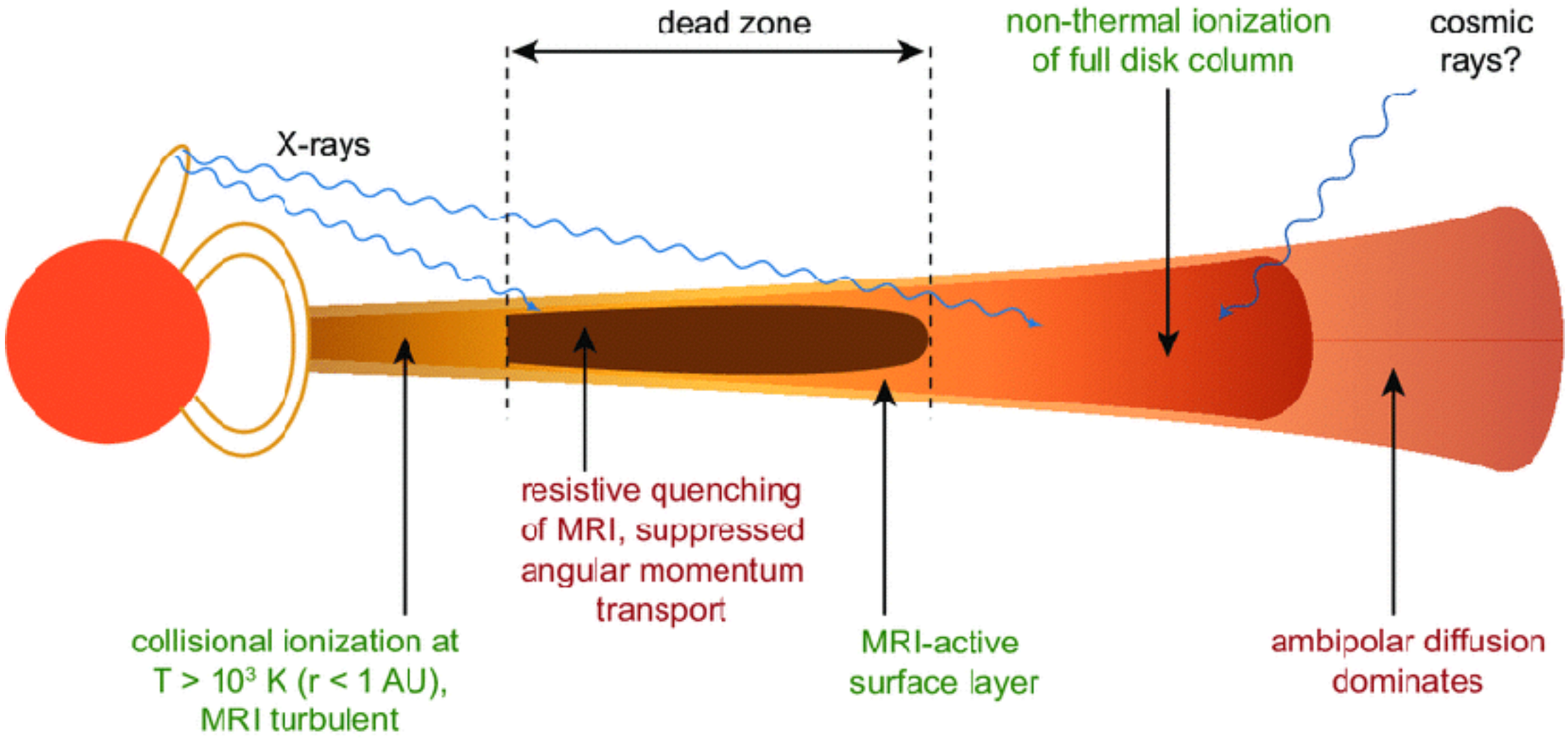

- Fleming & Stone 2003: MRI occurs only in the upper layers of the disks. The transport is maintained by velocity fluctuations in the center of the disk. CHANGES THE CONCEPT of DEAD ZONE
- Salmeron & Wardle 2003, 2004: hall effect and ambipolar diffusion change the growth of fluctuations at the mid plane, enhancing the transport at the midplane.
- Mori et al. 2019: the effect of radiation in the vertical structure of non ideal coefficients.
- Faure and Nelson 2015: planet trapping and migration, planet filtering by the transition (dead/ turbulent) surface.

Outline

- A setup for a local, non stratified protoplanetary disk to study of the transition between the active and ohmic dead zone in the radial direction.
- The ideal case: saturation and stress tensor, force balance.
- Saturation, stress tensor and force balance in a simulation with a resistivity profile which varies with R.
- Density accumulation and ring formation in a local system.
- Do spectral features of the magnetic field vary in the transition between active and resistive domains?

What I will not talk about

- Non isothermal equation of State (ask Matt Coleman) and radiative losses (e.g. Faure et al (2014)).
- Vertical stratification (Ambipolar diffusion e.g. Desch (2004)).
- The Hall effect (Bai and Stone (2017)) was found to respectively enhance or reduce the stresses and wind transport, depending on the disk vertical magnetic field being aligned or antialigned with respect to the angular momentum of the disk.
- Disk Chemistry (see e.g. Ilgner and Nelson (2006))
- Dust grain shape functions (Desch and Turner (2015))

Vertical resistivity profile

$$\eta = 6.5 \times 10^3 \chi^{-1} cm^2 s^{-1}$$ Hayashi 1981

Poloidal field no net flux MRI activation

$$Re_m = c_s^2/\Omega\eta > 10^4$$ Sano et al. 1998, Fleming et al. 2000

$$\eta(z) = \eta_0 exp\left(-\frac{z^2}{2}\right) exp\left(\frac{\Sigma_0}{\Sigma_{CR}}\right) \frac{1}{2\sqrt{\pi}} \int_z^\infty e^{-z'^2} dz' \qquad \Sigma_{CR} = 100 g cm^{-2}$$

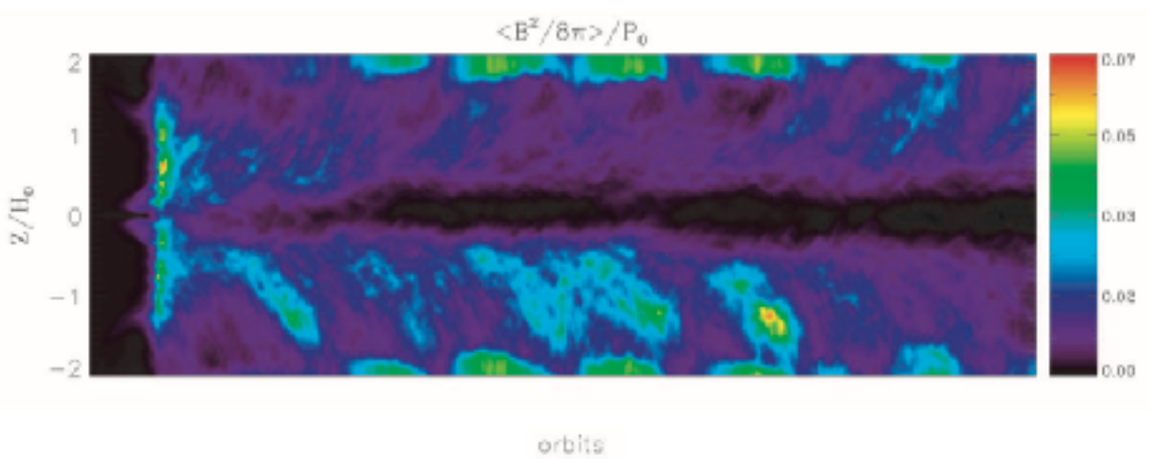

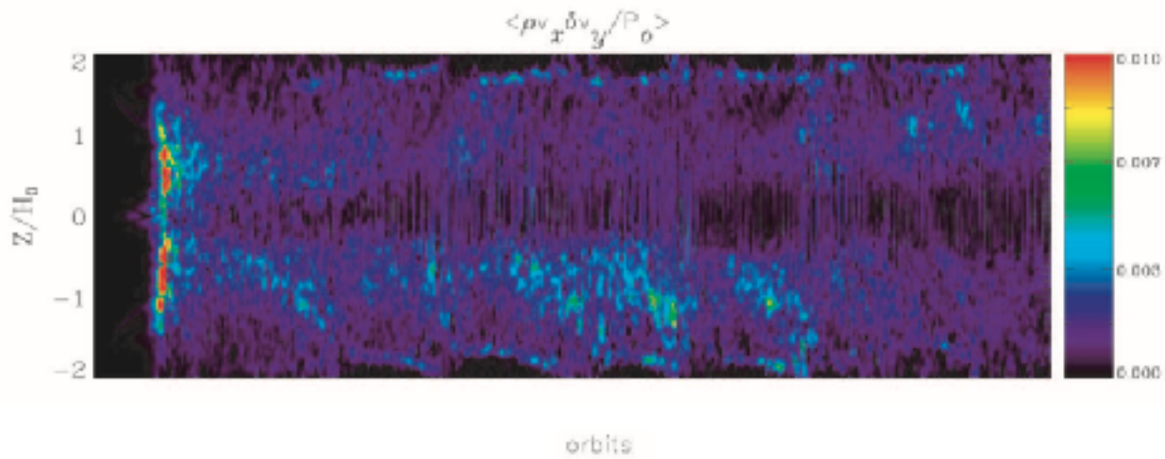

Fleming & Stone 2003

The shearing Box: Initial conditions

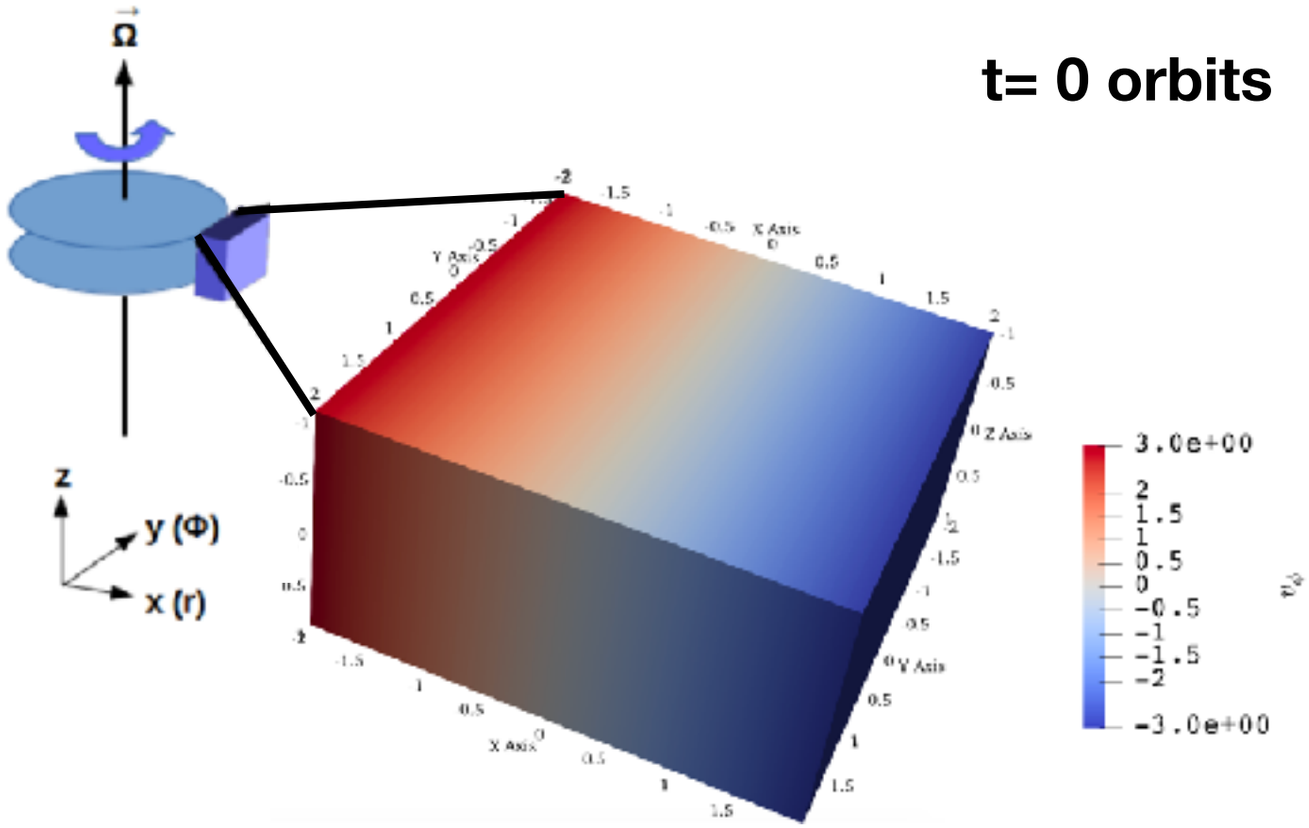

t= 0 orbits

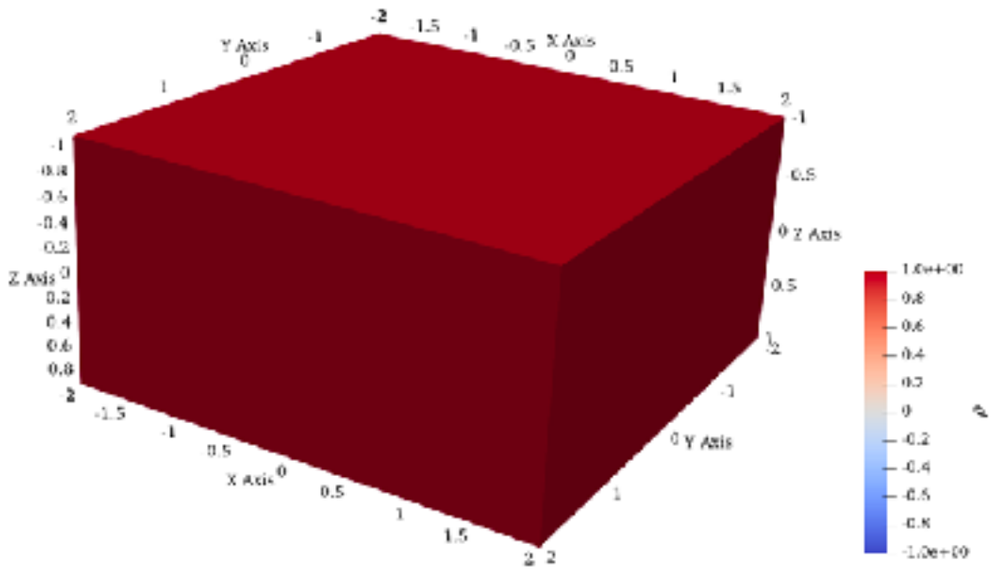

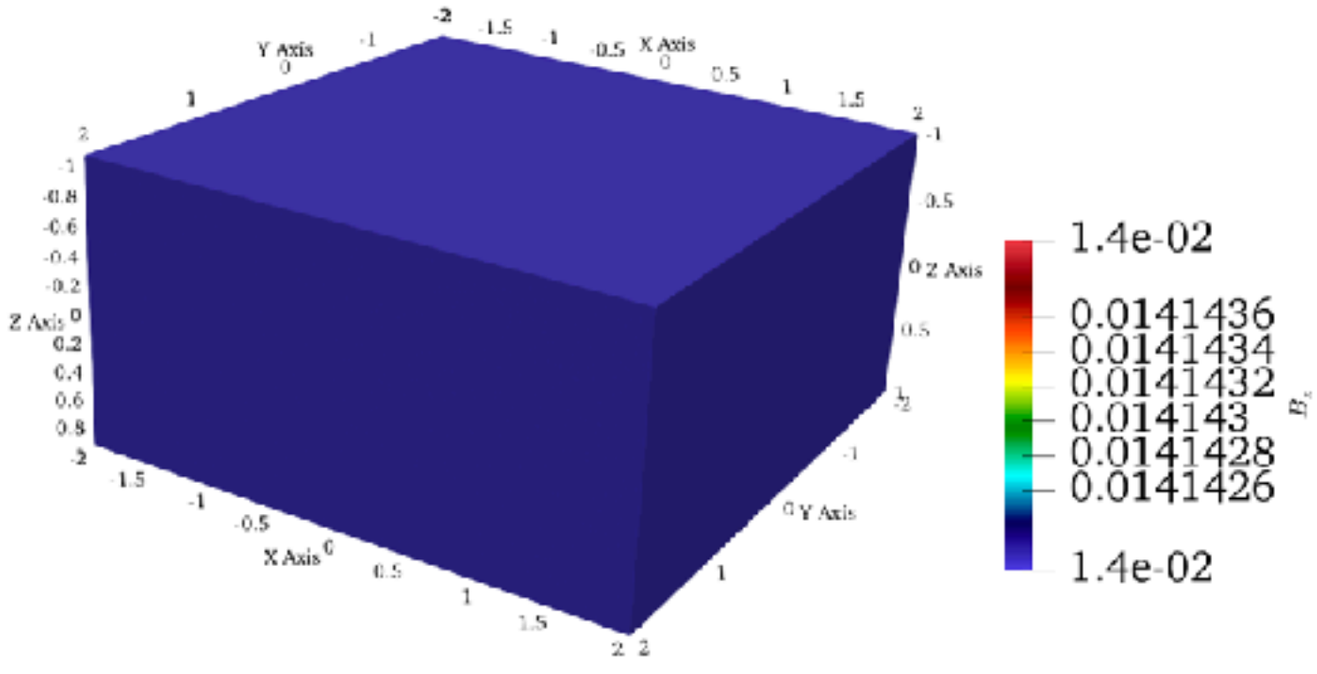

Vertical constant weak B field along z direction

$$P(t)\rho(t) = cost$$

$$B_{0z} = \sqrt{2P_0/\beta_0}$$

$$\beta_0 = 10^4$$

$$P_0 = 1, \rho_0 = 1$$

The shearing box equations and the angular Momentum transport

$$\frac{\partial \rho}{\partial t} + \nabla \cdot (\rho \boldsymbol{v}) = 0 \ ,$$

$$\frac{\partial \boldsymbol{v}}{\partial t} + \boldsymbol{v} \cdot \nabla \boldsymbol{v} = -\frac{1}{\rho} \nabla \left(P + \frac{B^2}{8\pi} \right) + \frac{\boldsymbol{B} \cdot \nabla \boldsymbol{B}}{4\pi\rho}$$

$$- 2\Omega \times \boldsymbol{v} + 3\Omega^2 x \hat{\boldsymbol{x}} - \Omega^2 z \hat{\boldsymbol{z}}$$

$$\frac{\partial \boldsymbol{B}}{\partial t} = \nabla \times [(\boldsymbol{v} \times \boldsymbol{B}) - \eta(x) \boldsymbol{J}] \ ,$$

$$P = c_s^2 \rho \ ,$$

$$h = r^2 \Omega$$

$$\mathcal{F} = 2\pi r \bar{u}_r$$

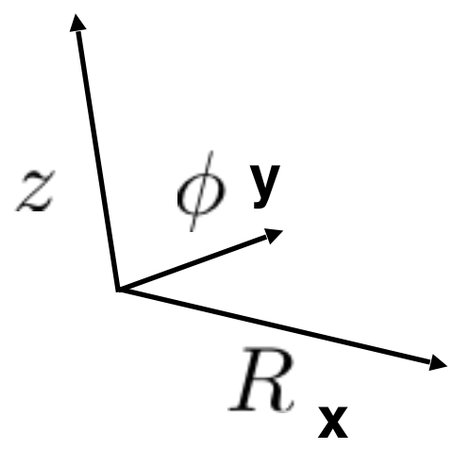

$$\partial_r h \, \mathcal{F} = \partial_r \int_0^{2\pi} \int_{-\infty}^{\infty} \partial_r r^2 T_{r\phi} dz d\phi$$

Hawley, Gammie, Balbus 1995

$$\lambda_C = 9.18 \beta^{-1/2}$$

Ideal configuration

Periodic boundaries in z, shear periodic in x, periodic in y

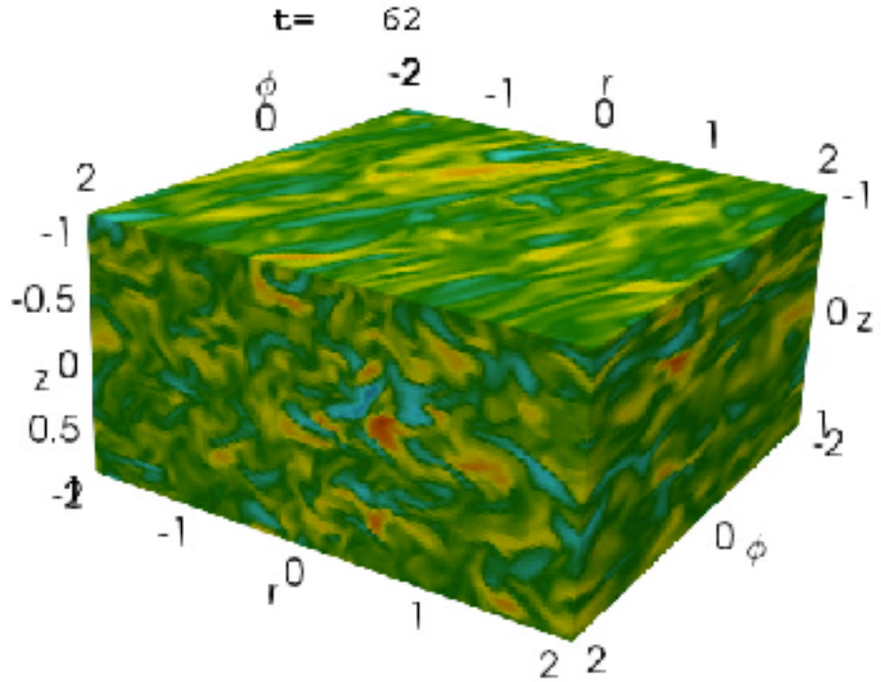

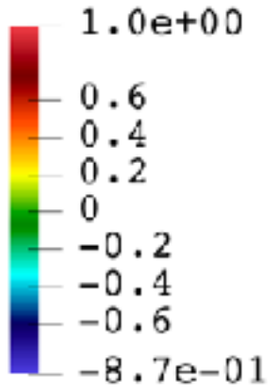

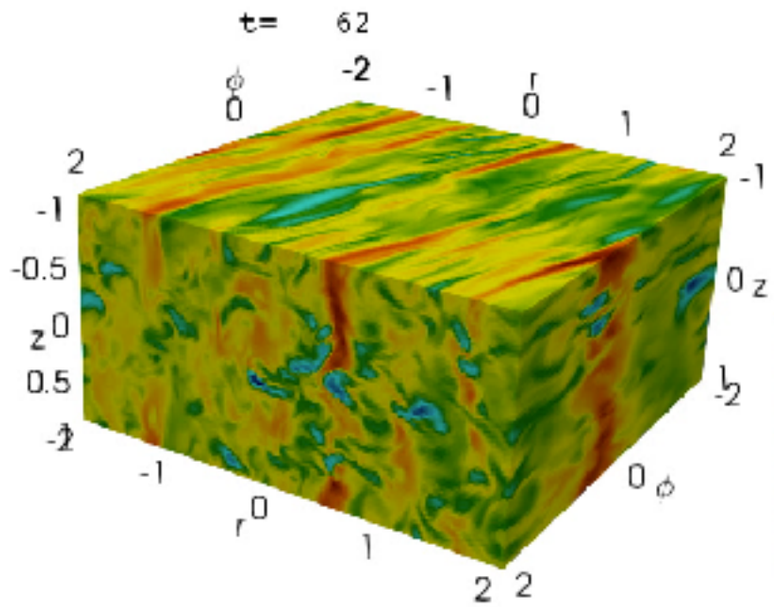

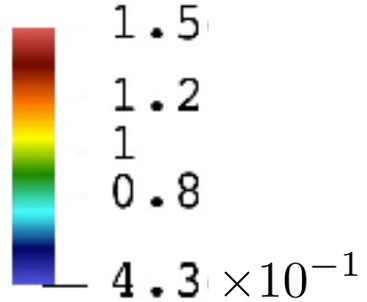

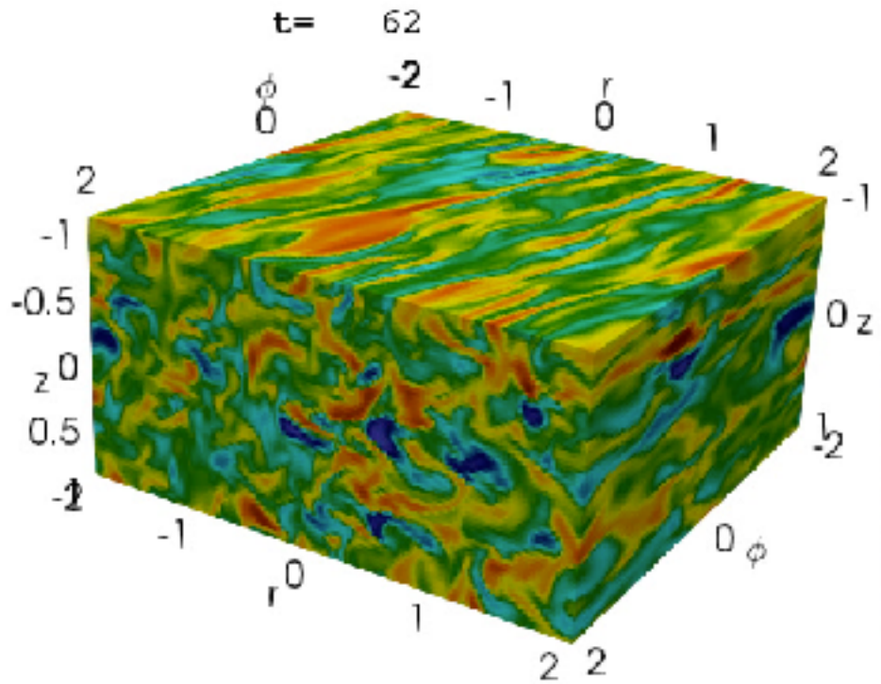

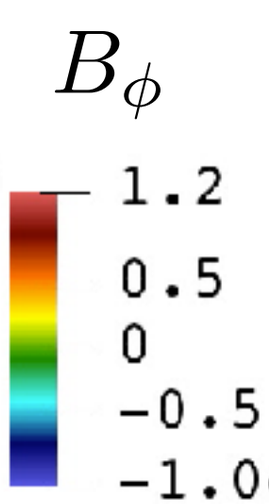

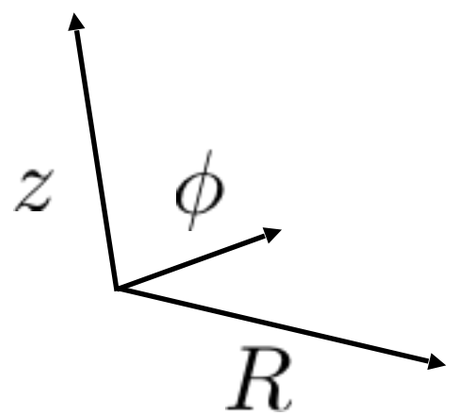

Stress Tensor

From, e.g. Stone and Gardiner 2010

azimuthal velocity fluctuations $v_y + q\Omega_0 x$

$$\mathbf{v}_K = -q\Omega_0 x\hat{\mathbf{j}}$$

Shear at t=0 in ϕ

Normalization and actual calculation. From Shi et al 2015:

$$\alpha_{\rm M} \equiv \langle\langle -\frac{B_x B_y}{4\pi P_0}\rangle\rangle_t \,, \alpha_{\rm R} \equiv \langle\langle \frac{\rho v_x \delta v_y}{P_0}\rangle\rangle_t$$

Setup 1:ideal

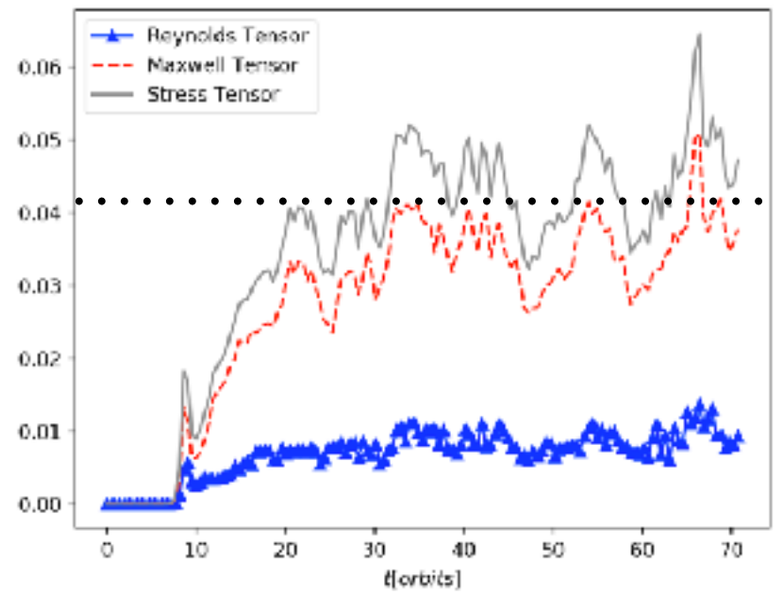

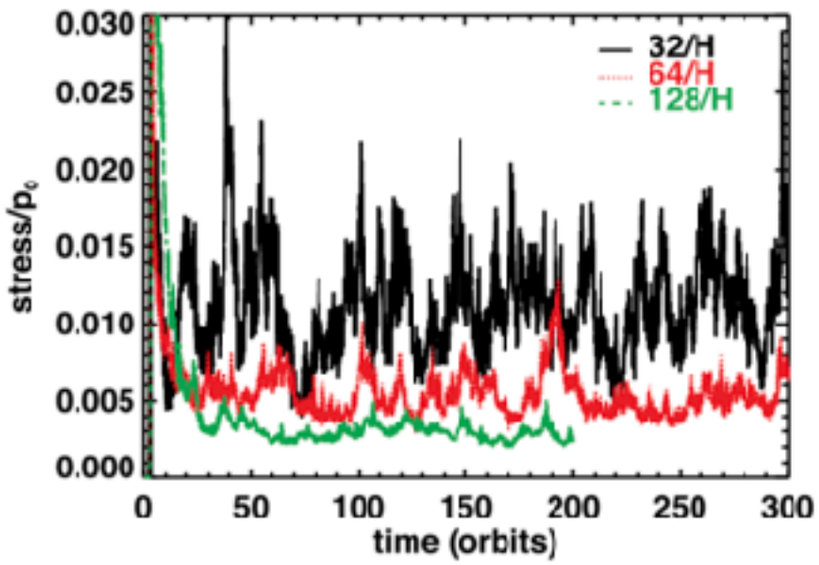

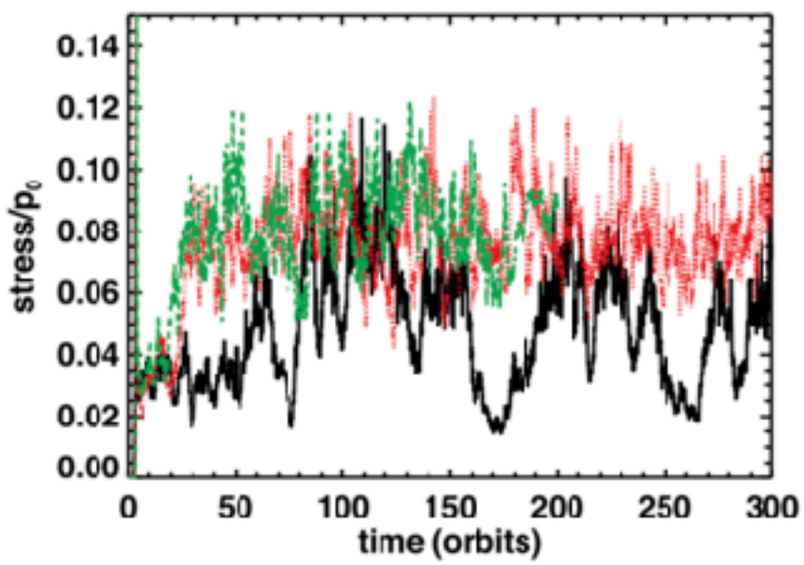

$$q = -\frac{1}{2}\frac{dln\Omega^2}{dlnr} = \frac{3}{2}$$

Figure 2. The volume-averaged stresses for a standard box ($(L_x, L_y, L_z) = (1, 4, 1)H$, left-hand panel) and a tall box ($(L_x, L_y, L_z) = (1, 4, 4)H$, right) with various resolutions: $32/H$(black solid),$64/H$(red dotted) and $128/H$(green dashed). In contrast to the small box, the vertically elongated box achieves good convergence.

Setups

Name	N_x	N_y	N_z	η	β	L_x	L_y	L_z	$T[Orbits]$
Setup1	256	128	64	0	10^4	4	4	2	~ 70
Setup2	256	128	64	10^{-2}	10^4	4	4	2	~ 70

$$\eta(r) = \frac{\eta_0}{2}(\tanh((r+1)/a) - \tanh((r-1)/a));$$

$$a = 0.1$$

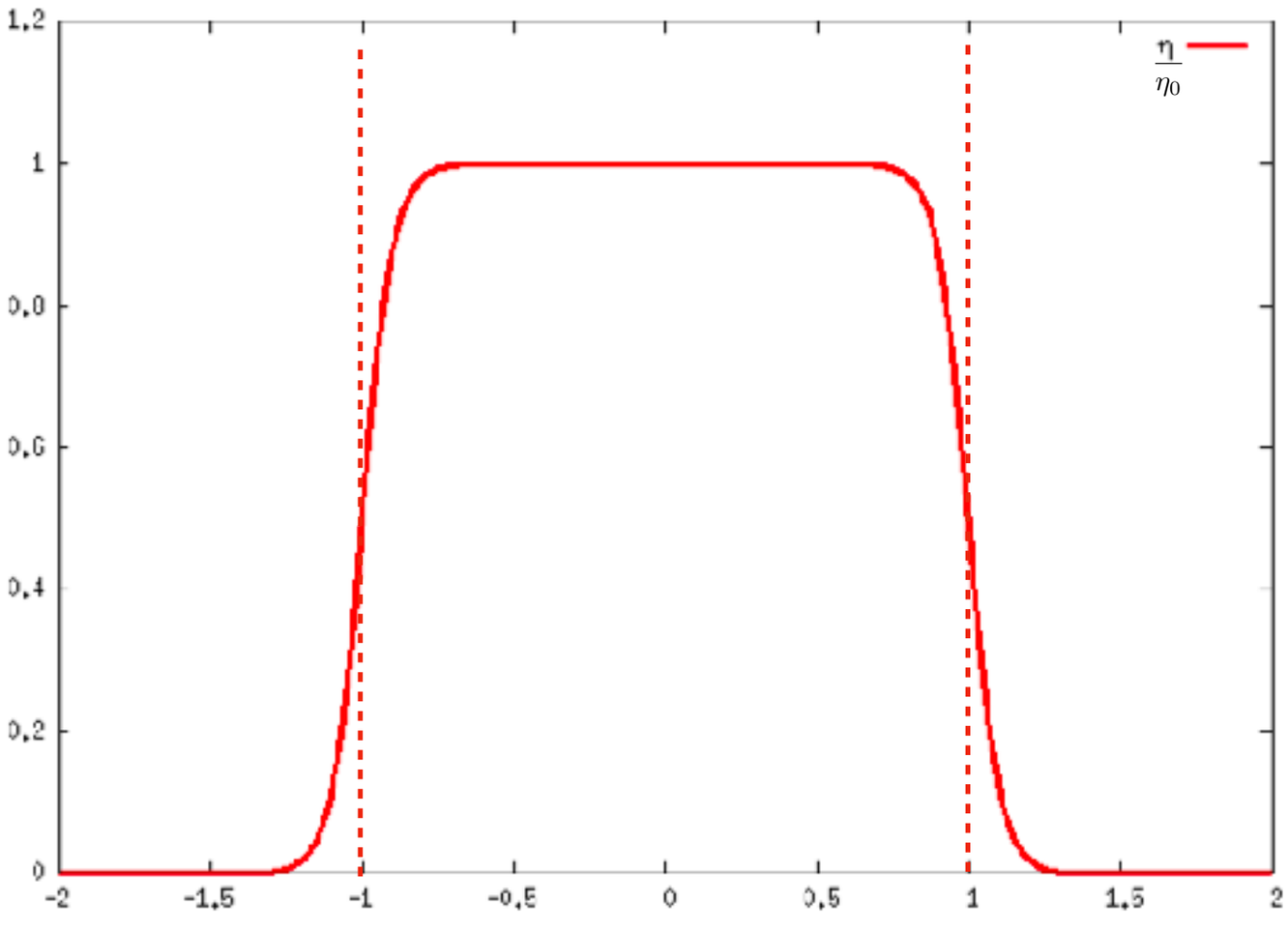

Blaes, Balbus 1994

$$\nu_c = \alpha^i n_i \left(1 + \frac{\alpha^i}{\alpha^a}\frac{1-\chi}{\chi}\right)$$

$$\chi = \frac{n_i}{n_a + n_i}$$

$$\alpha = \sigma\bar{v}$$

$$\nu_c > \nu_{epi}(r,\phi,z) = 4\Omega^2 + \frac{\partial\Omega^2}{\partial lnr}$$

$$r = 1AU, n = 10^{13}cm^{-3} \Rightarrow \chi = 10^{-11}$$

Setup2: Beta=10^4 $\eta = 10^{-2}$

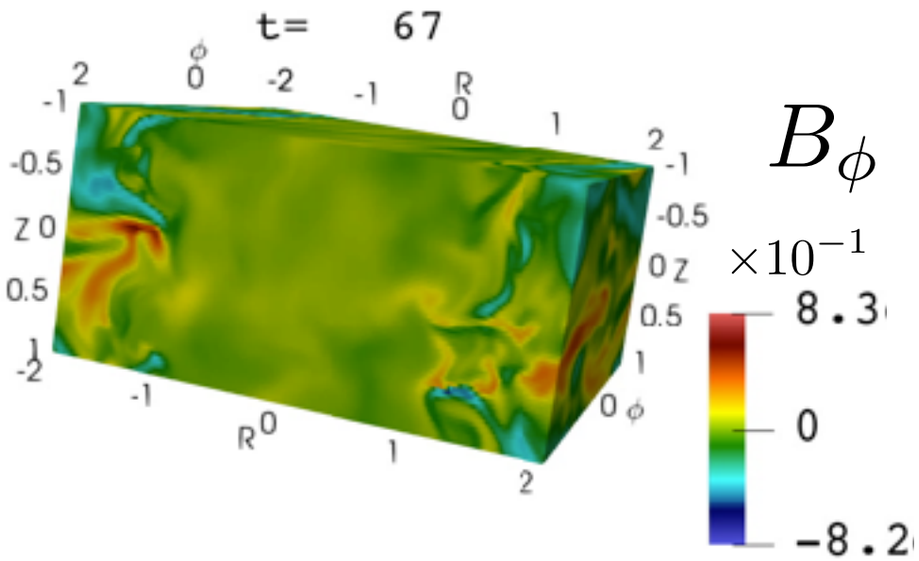

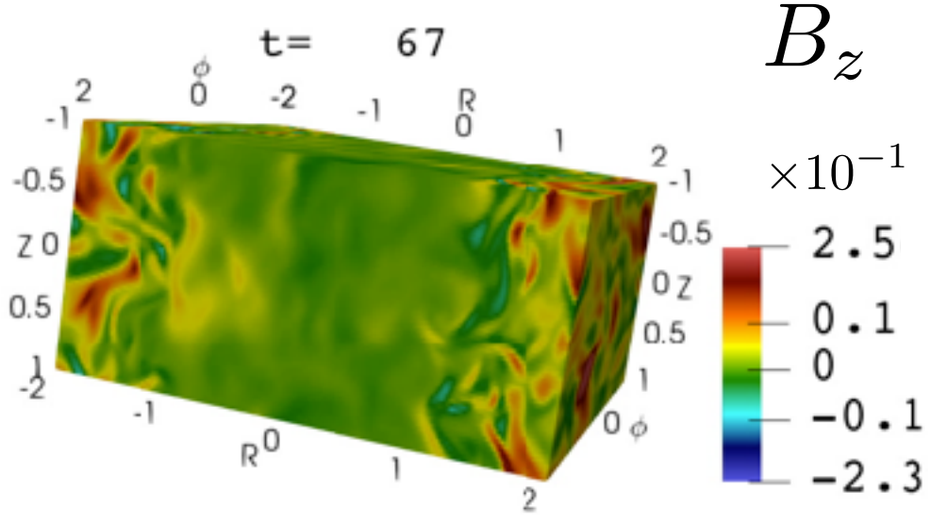

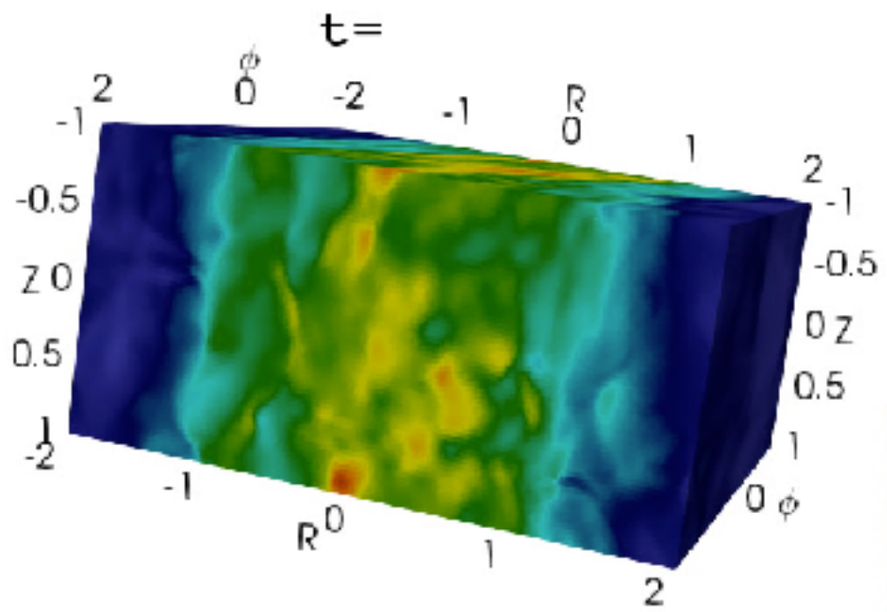

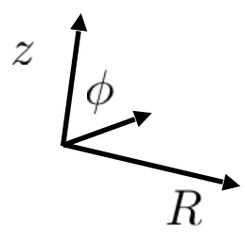

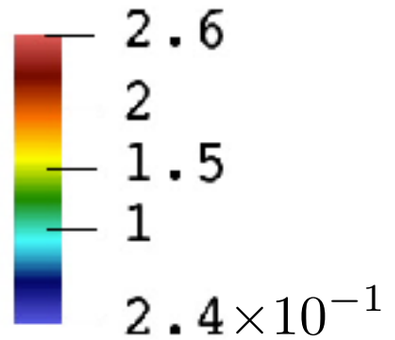

2D profiles : resistive vs ideal case, stress tensor

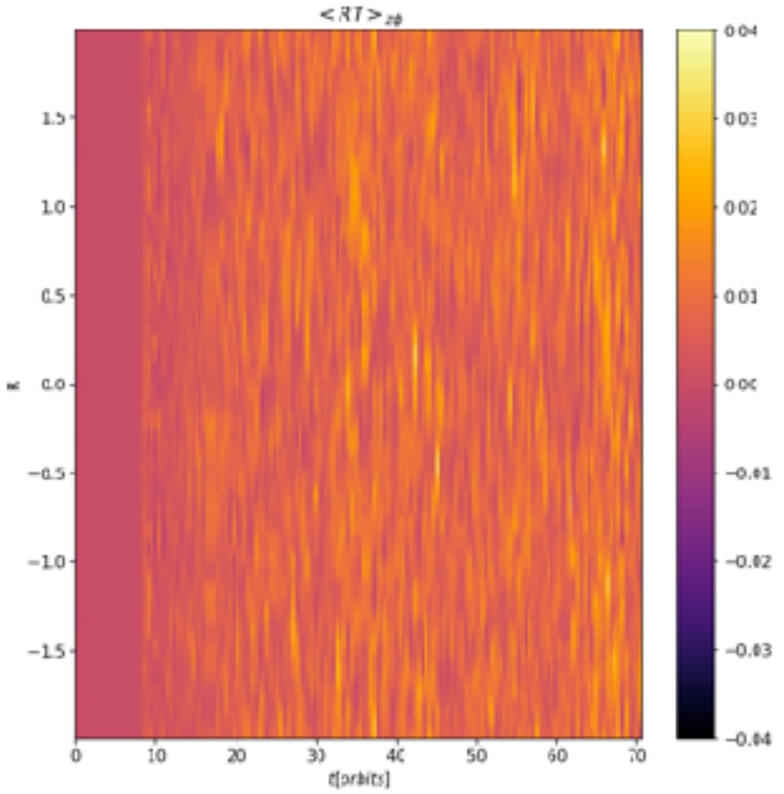

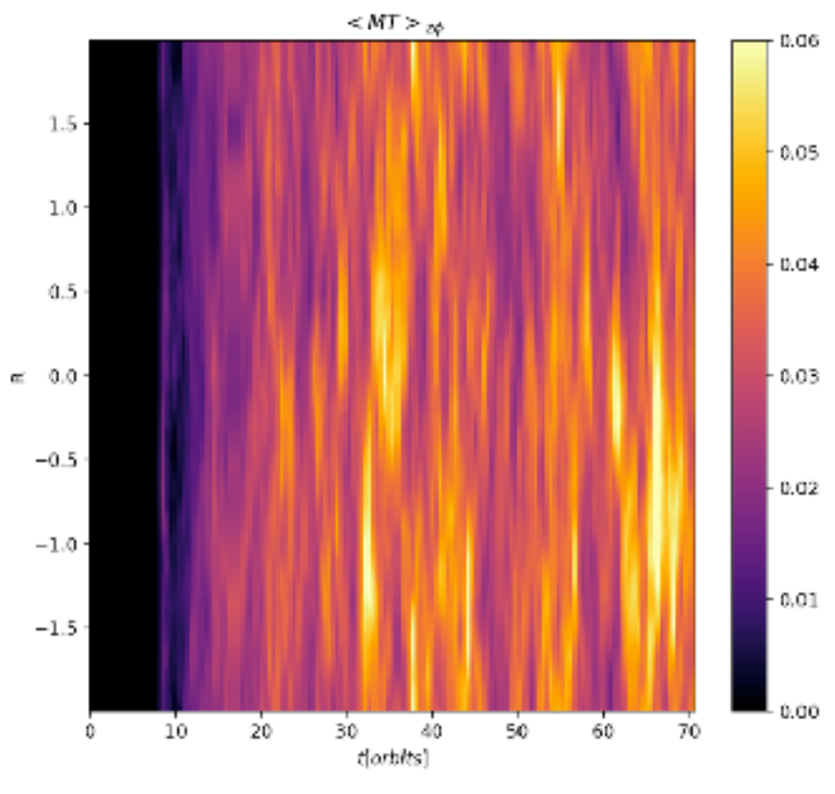

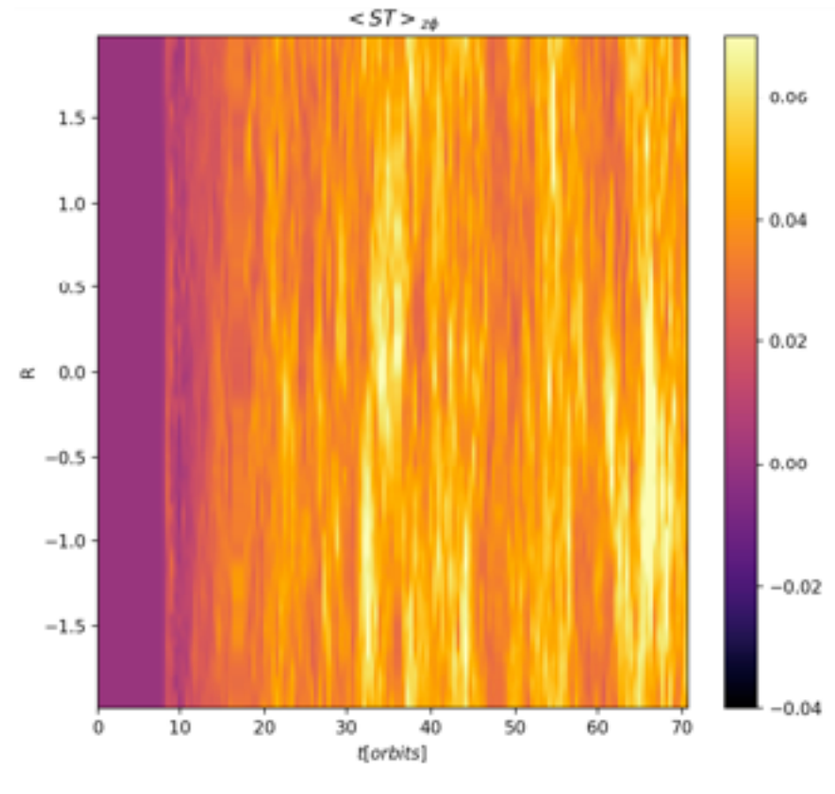

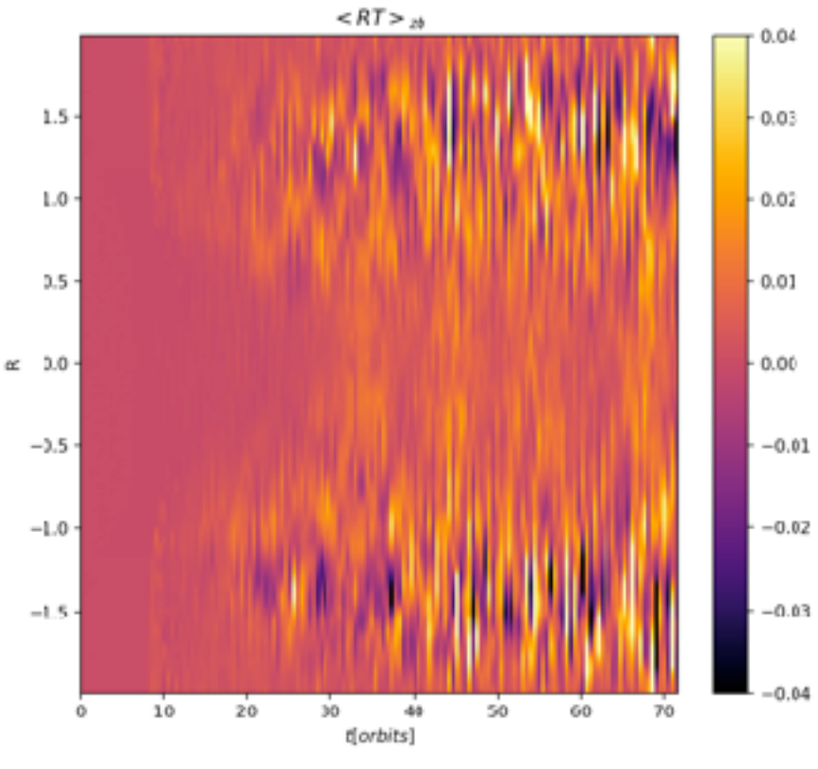

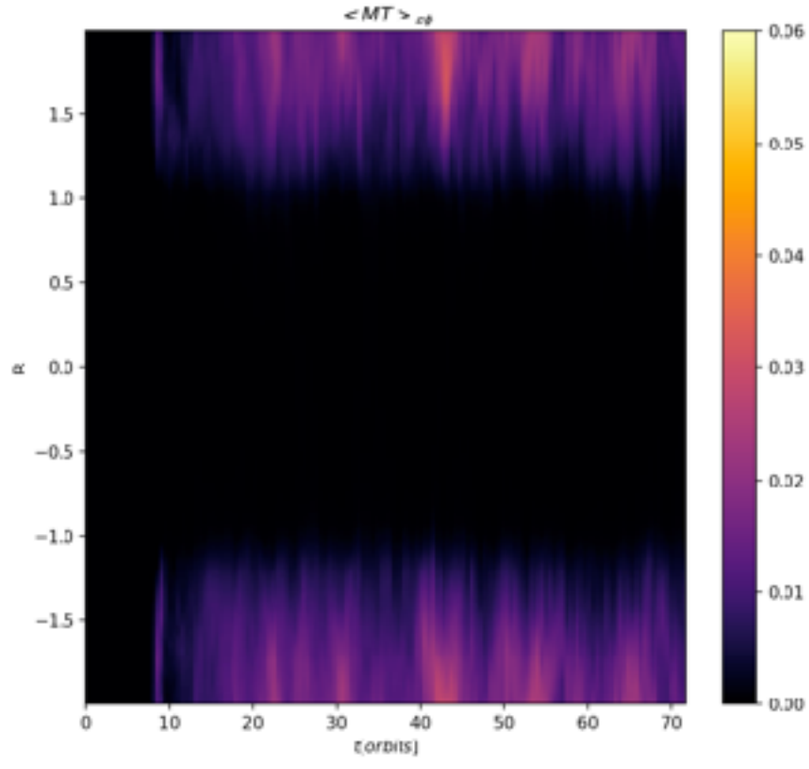

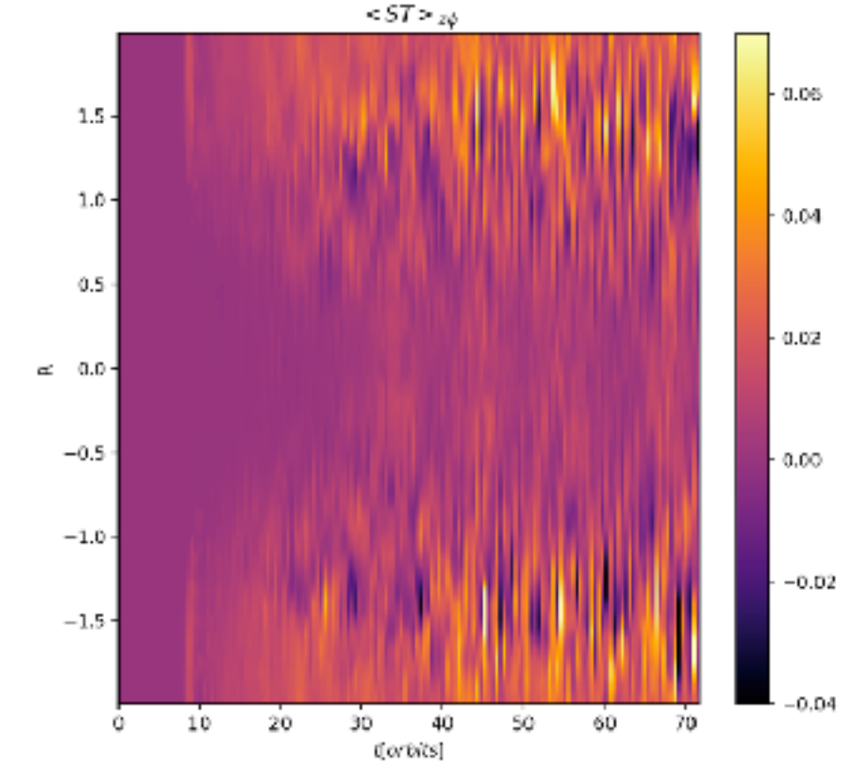

Ideal configuration: Force balance

$$\frac{\partial \rho}{\partial t} + \nabla \cdot (\rho \boldsymbol{v}) = 0 \ , \tag{1}$$

$$\frac{\partial \boldsymbol{v}}{\partial t} + \boldsymbol{v} \cdot \nabla \boldsymbol{v} = -\frac{1}{\rho} \nabla \left(P + \frac{B^2}{8\pi} \right) + \frac{\boldsymbol{B} \cdot \nabla \boldsymbol{B}}{4\pi\rho} - 2\Omega \times \boldsymbol{v} + 3\Omega^2 x \hat{\boldsymbol{x}} - \Omega^2 z \hat{\boldsymbol{z}} \ , \tag{2}$$

$$\frac{\partial \boldsymbol{B}}{\partial t} = \nabla \times [(\boldsymbol{v} \times \boldsymbol{B}) - \eta(z) \boldsymbol{J}] \ , \tag{3}$$

$$P = c_s^2 \rho \ , \tag{4}$$

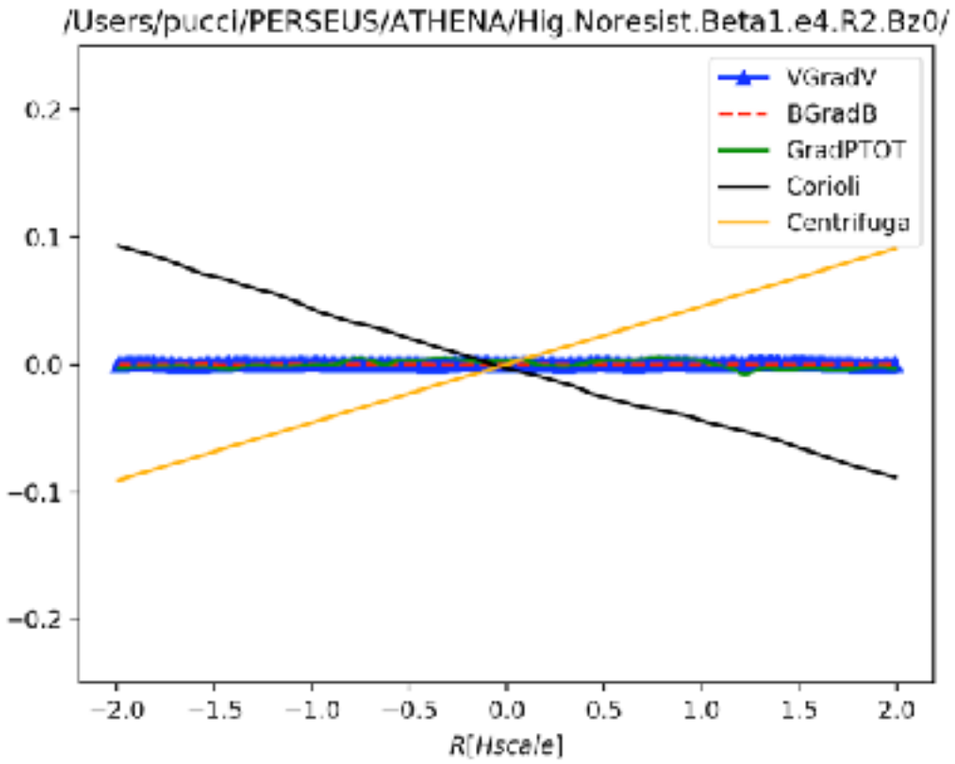

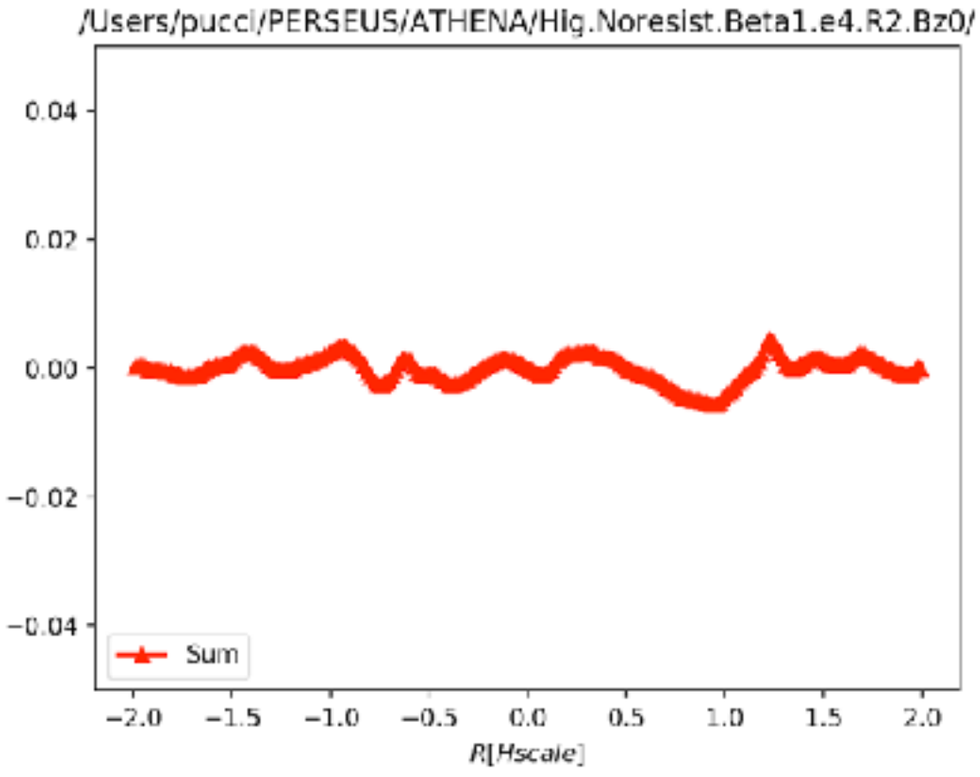

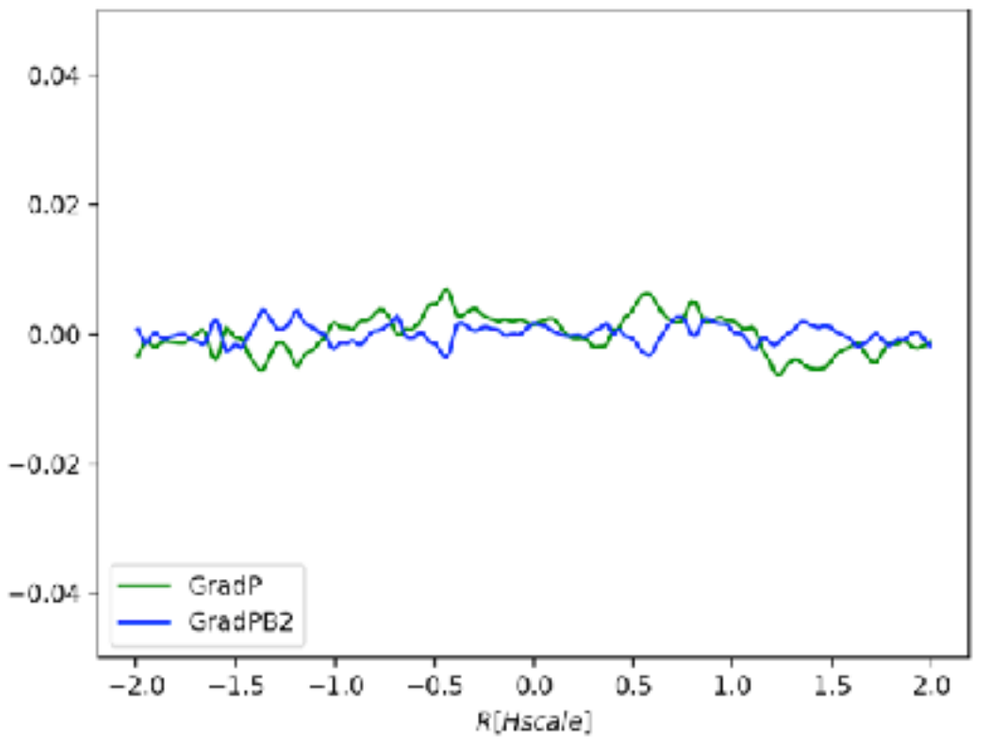

Setup2: Beta=10^4, force balance $\eta = 10^{-2}$

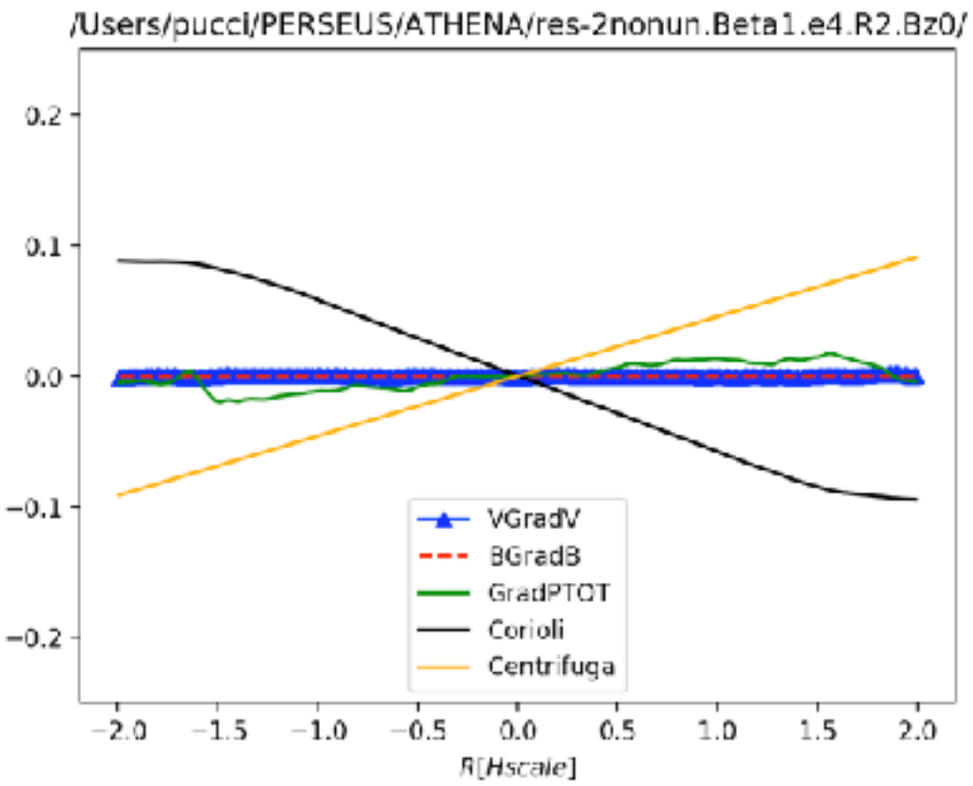

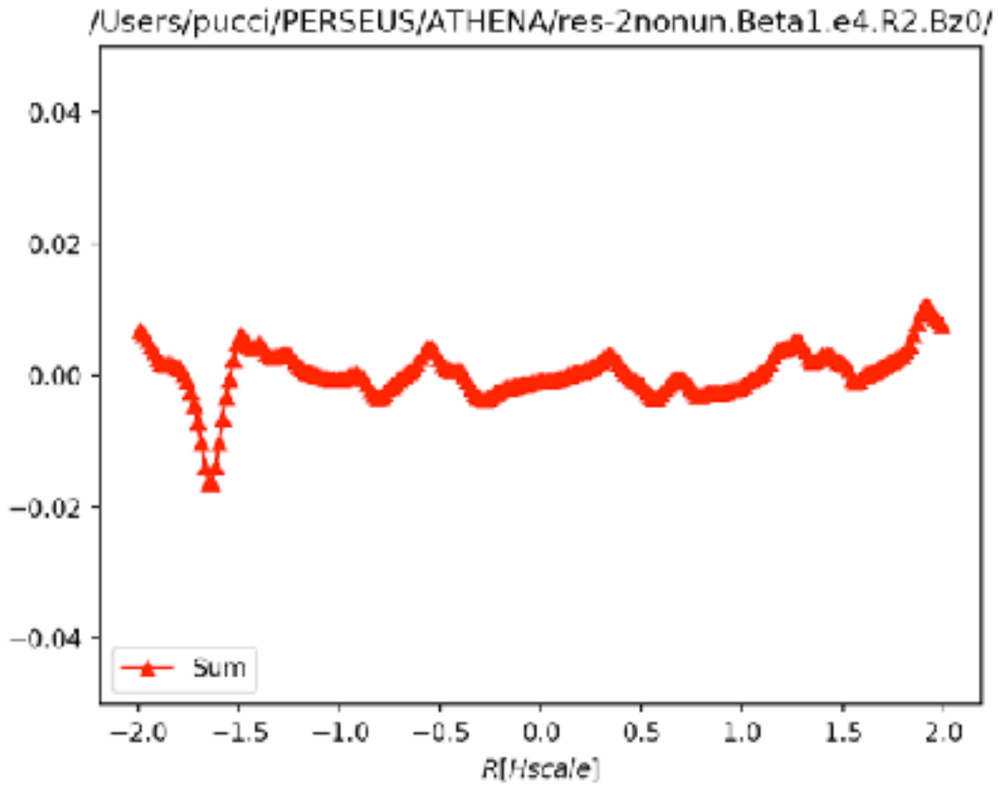

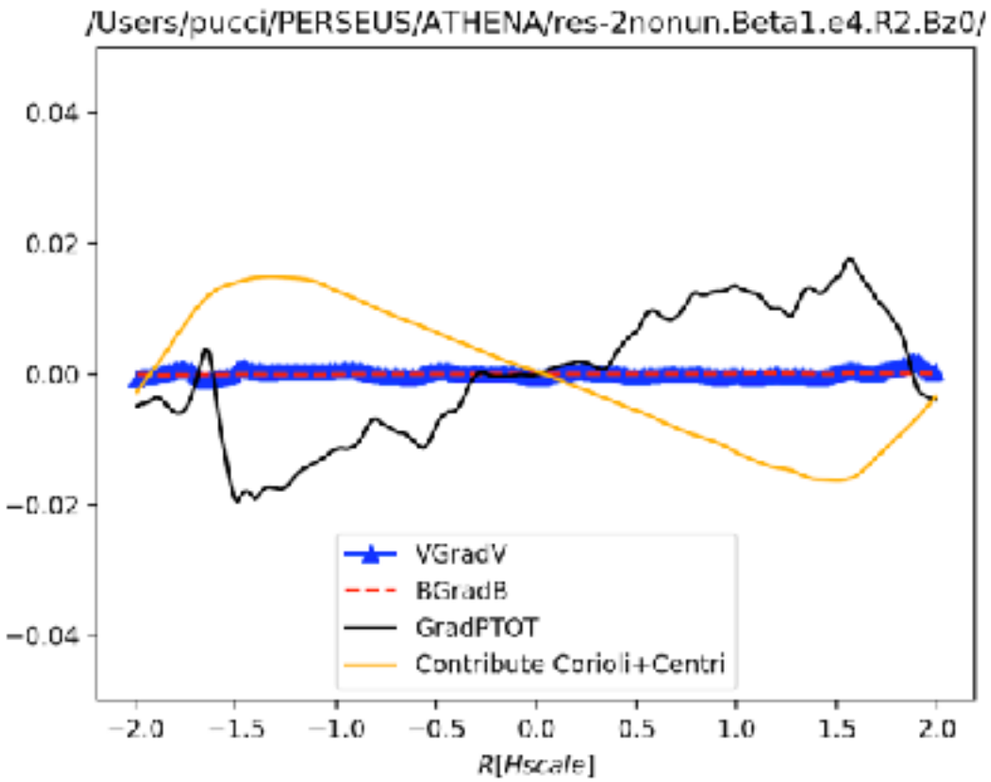

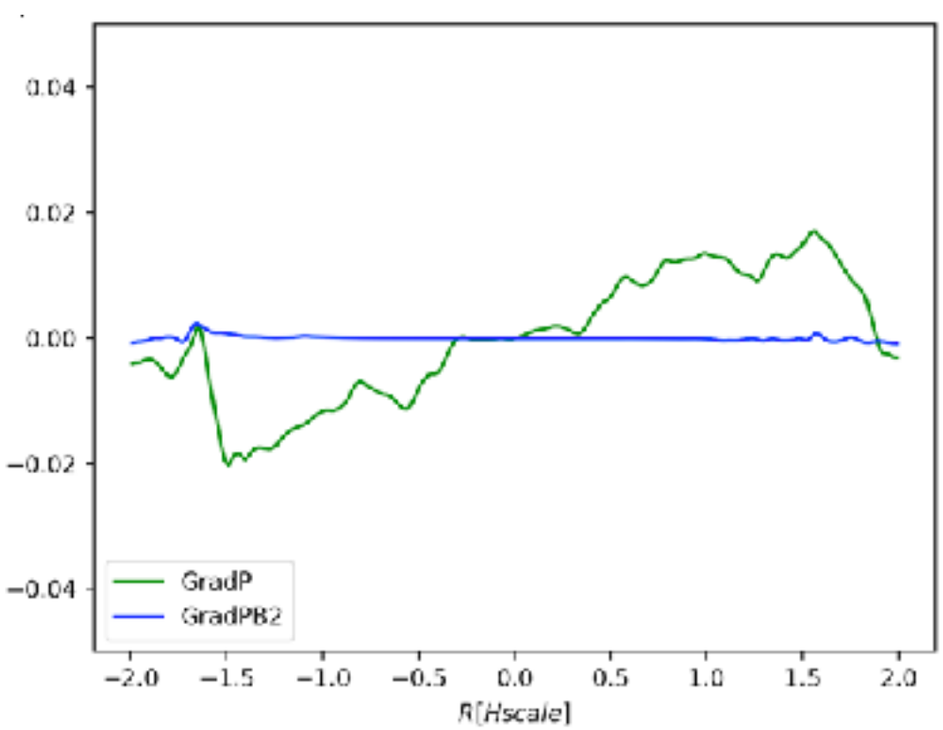

Density bump and azimuthal jets

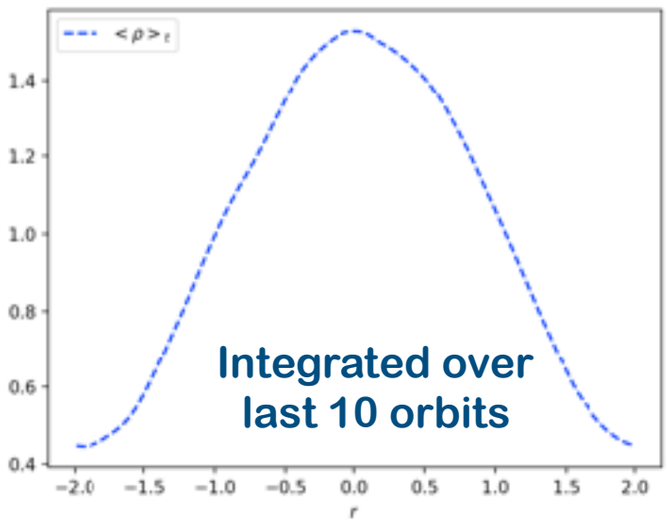

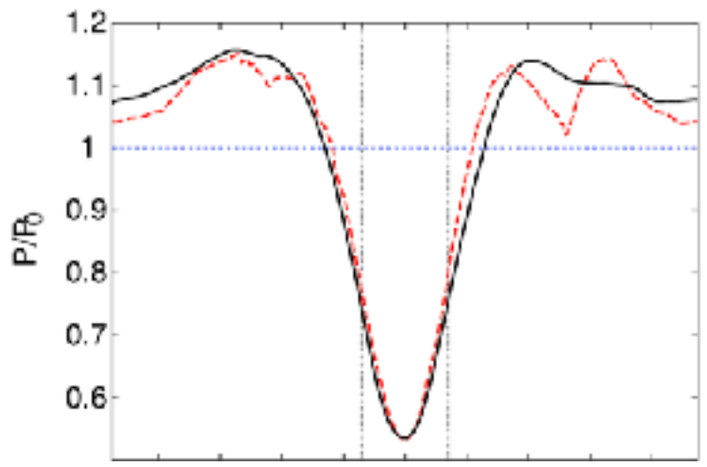

Kato et al. 2012

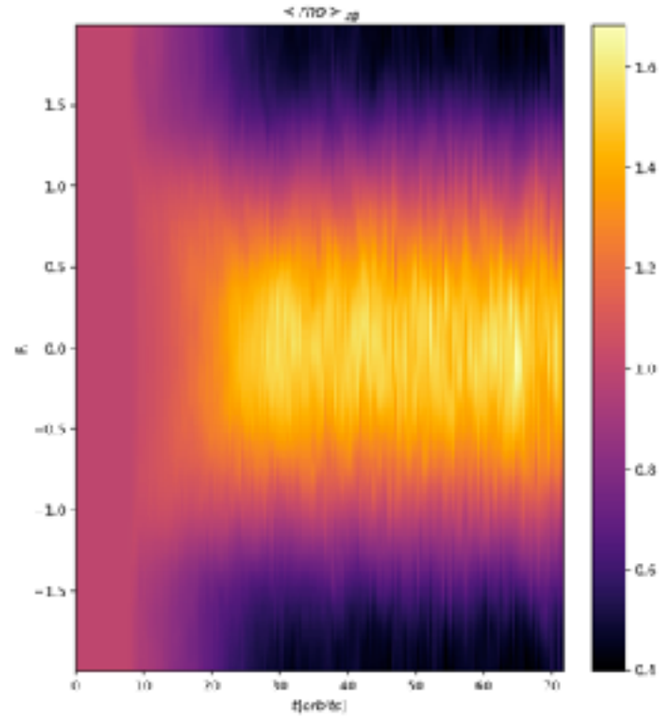

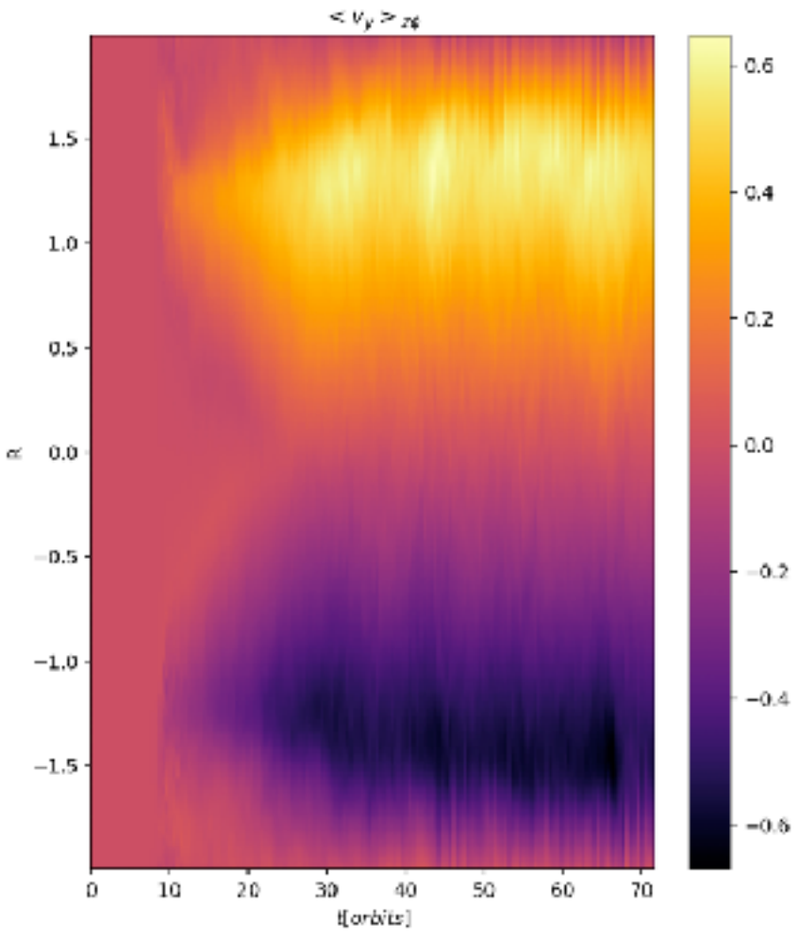

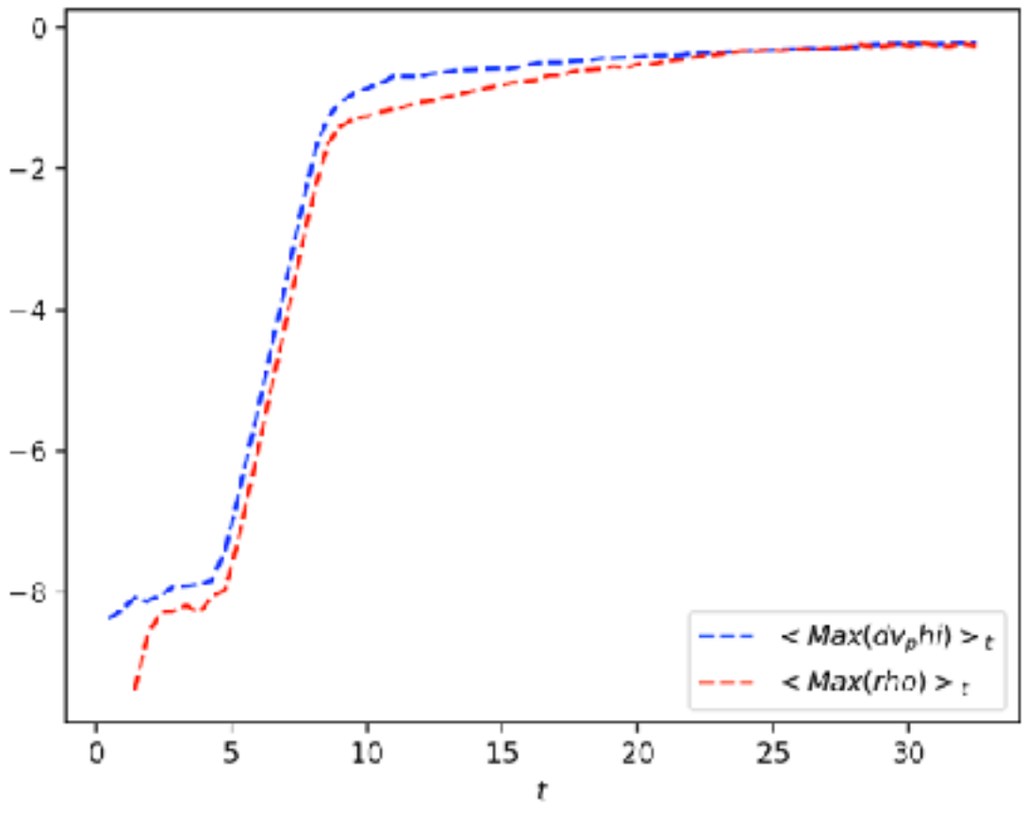

The viscoresistive corotation theorem

$$\vec{\nabla}\wedge\left(\begin{array}{c}\frac{4\pi}{c^2}\omega\partial_r\psi+\eta\frac{1}{r}\partial_z I\\ \frac{4\pi}{c^2}\left(v_r B_z-v_z B_r\right)+\eta\left[\frac{\partial_z^2\psi}{r}+\partial_r\left(\frac{\partial_r\psi}{r}\right)\right]\\ \frac{4\pi}{c^2}\omega\partial_z\psi-\eta\frac{1}{r}\partial_r I\end{array}\right)=0.$$

Axial symmetry

$$\vec{B}=\frac{1}{r}\vec{\nabla}\psi\wedge\hat{e}_\phi+\frac{I}{r}\hat{e}_\phi$$

$$\partial_r\psi=Cr$$

B slowly changing with time!

$$\frac{4\pi}{c^2}\left(\vec{\nabla}\omega\wedge\vec{\nabla}\psi\right)=\vec{\nabla}\wedge\left(\eta\frac{\vec{\nabla}I}{r}\wedge\hat{\phi}\right)$$

$\eta=0\Rightarrow\omega=\omega(\psi)$ **Function of the magnetic flux surface**

$\eta=O(1)$ **The Ferraro Theorem is valid depending on the order of**

$$\vec{\nabla}I$$

V. C. A. Ferraro, MNRAS, 97, 458 (1937)

R. Benini et al 2011 EPL 96 19002

2D profiles : resistive vs ideal case, magnetic field

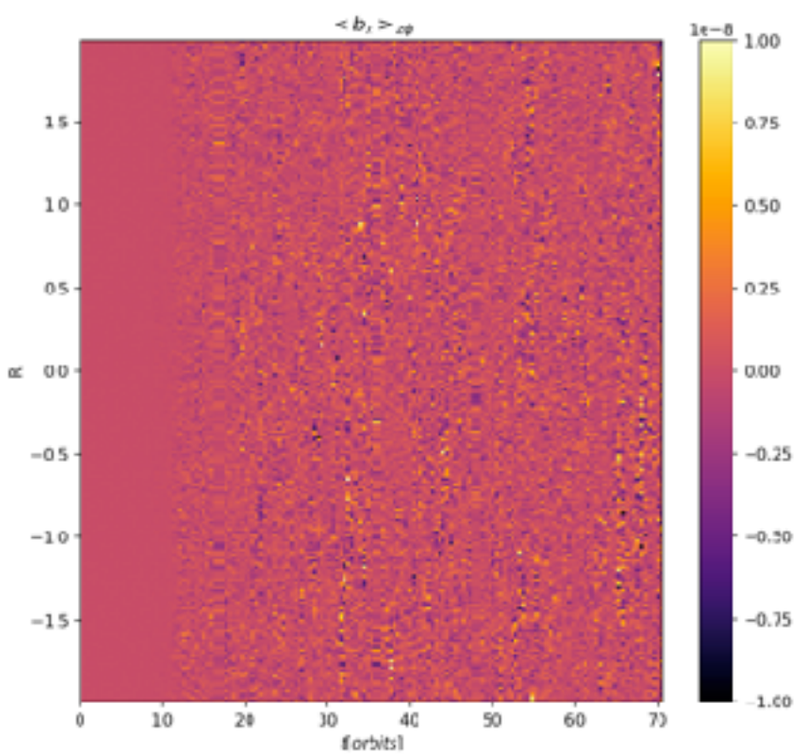

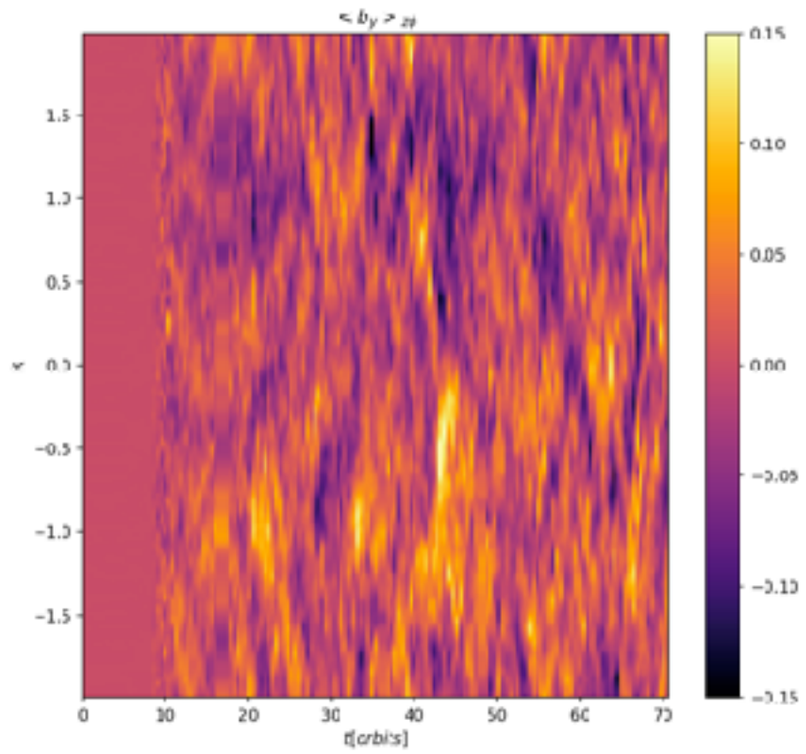

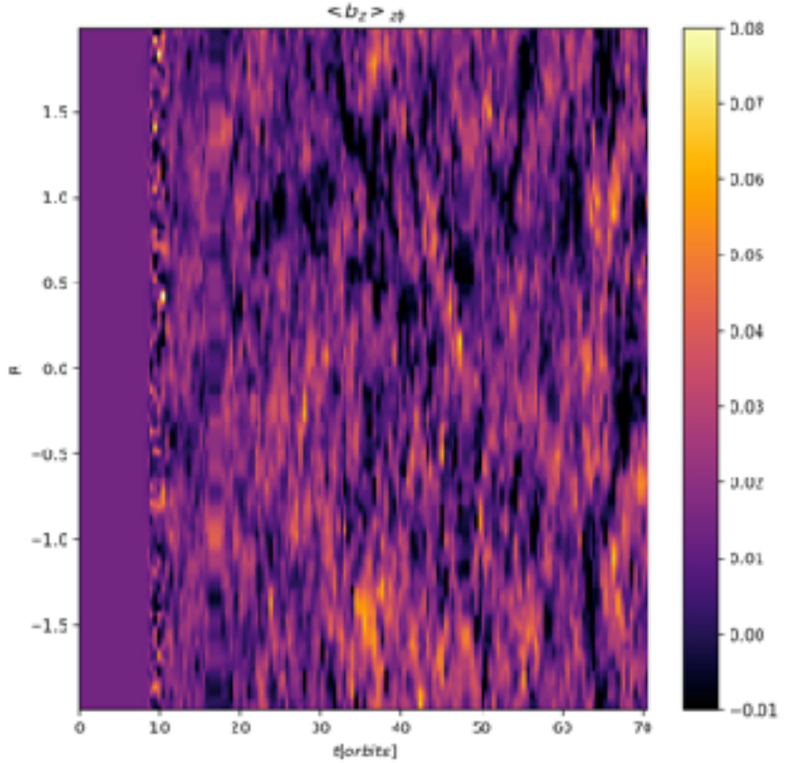

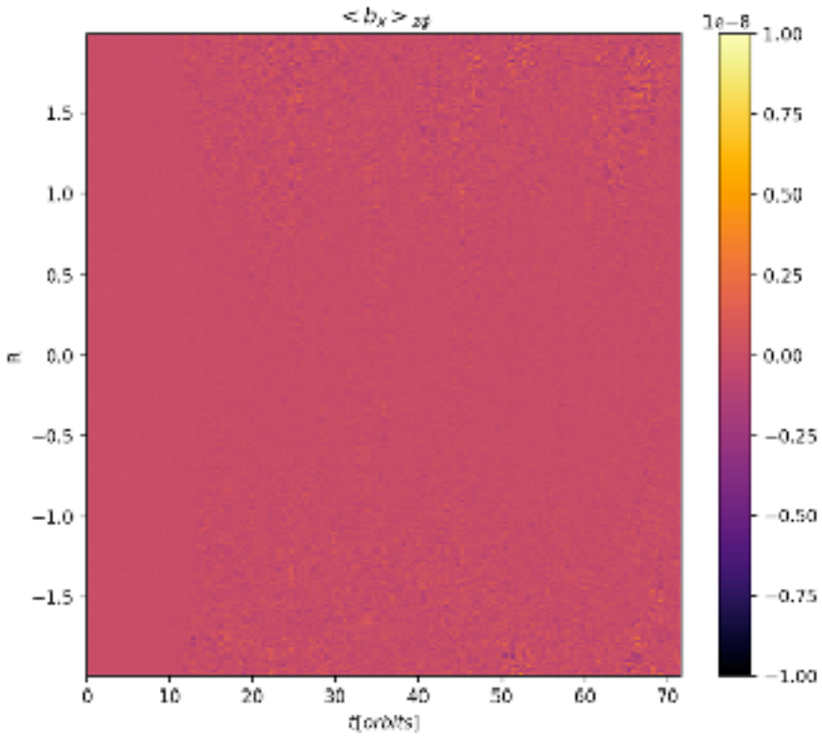

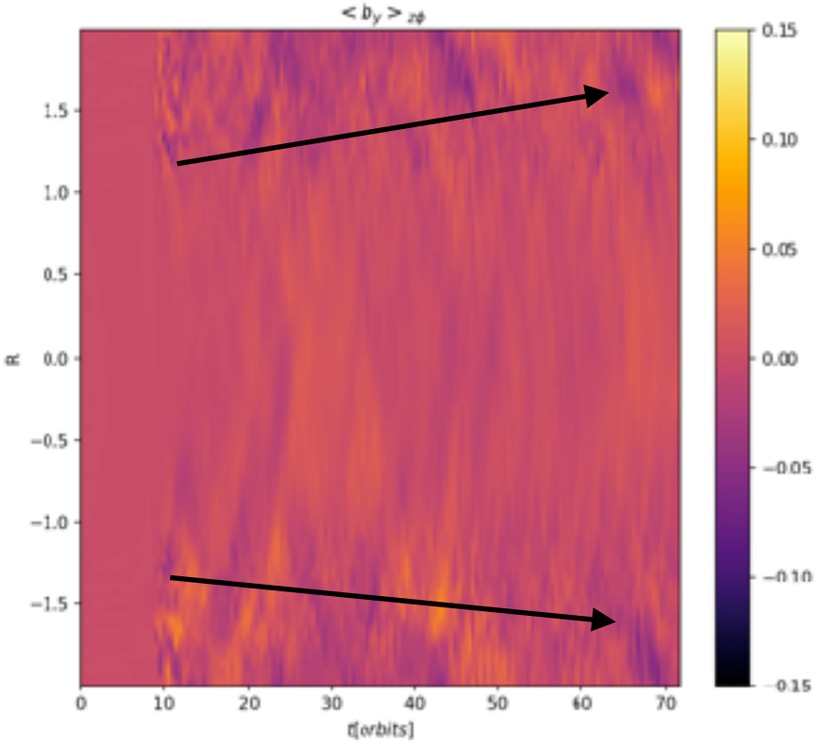

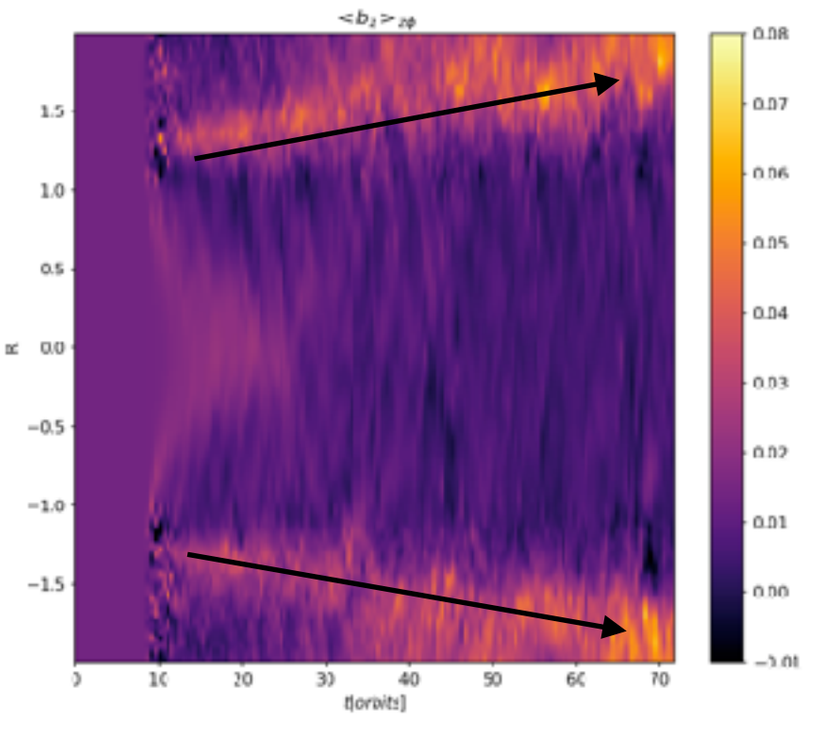

Solution of v_r for Prandtl # 1

$$\omega_{\mathrm{K}} \equiv \omega\left(\psi_0\right) = \sqrt{\frac{GM_*}{r_0^3}}$$

$$\vec{B} = \frac{1}{r}\vec{\nabla}\psi \wedge \hat{e}_\phi + \frac{I}{r}\hat{e}_\phi$$

$$\omega = \omega_{\mathrm{K}} + \omega_0' \psi_1 \qquad \omega_0' \equiv \left.\frac{\mathrm{d}\omega}{\mathrm{d}\psi}\right|_{\psi_0}$$

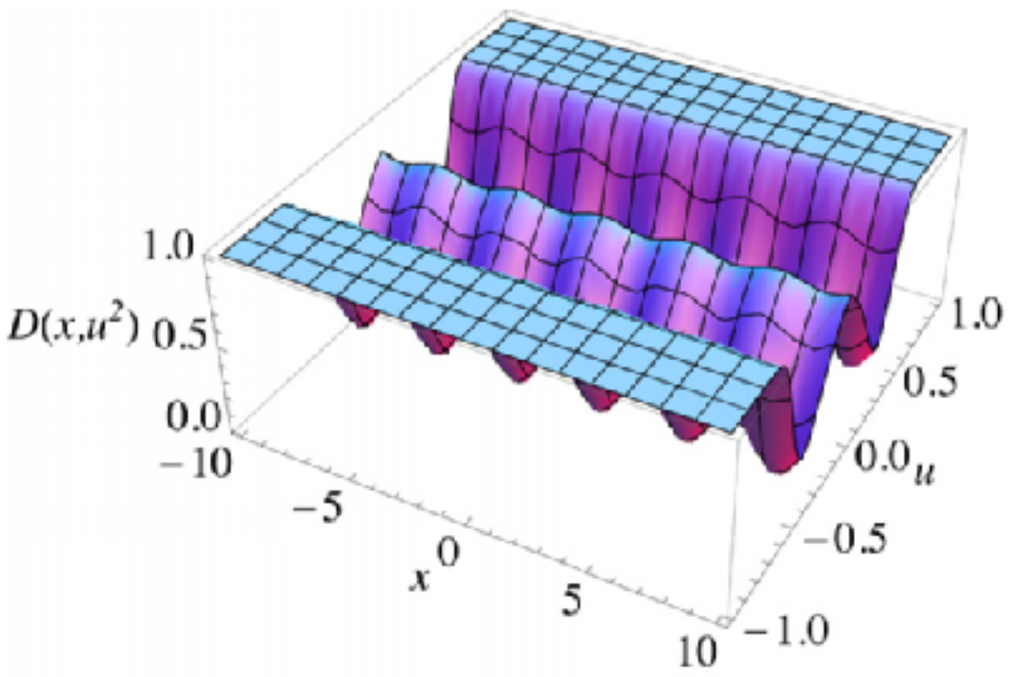

Fig. 1: (Colour on-line) 3D plot for the total density $D(x, u^2)$ (43), with parameters chosen as $A = 1\,, C = -1\,, a = -\sqrt{3}\,, b = -\frac{1}{6}\,, \varepsilon_z = 0.05\,, B = \sqrt{40}$. The density profile exhibits a modulation along the radial direction, while in the vertical direction two minima appear.

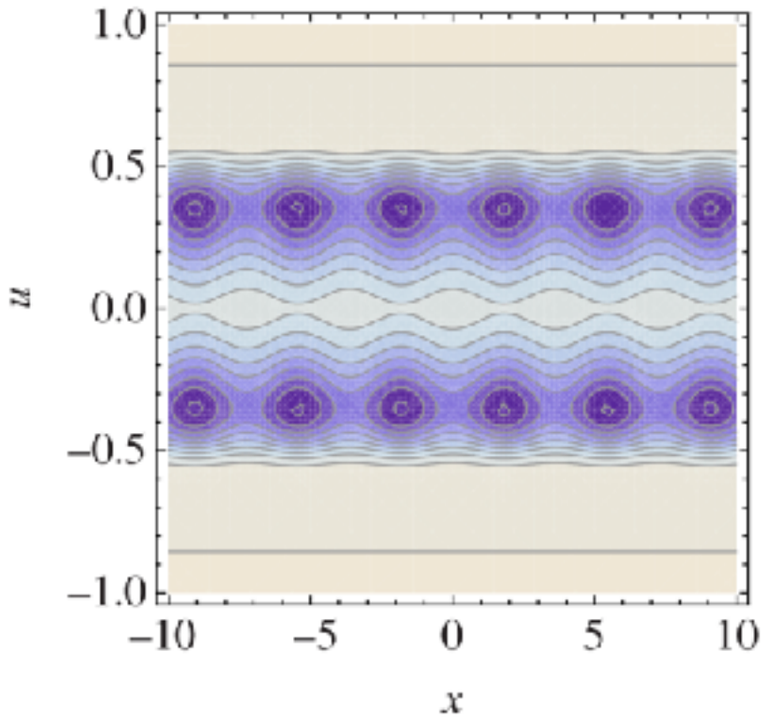

Fig. 2: (Colour on-line) Level lines for the total density $D(x, u^2)$ (43), with parameters chosen as in fig. 1. We note that the darkest zones are the minima of density, and the ring sequence appears in the equatorial plane.

Setup2: profiles of v² ,Beta=10⁴ , $\eta = 10^{-2}$

How to read the spectra?

The line color correspond to the x1 value where the fft is calculated in the graph below

This cube of data is at t=47.75[orbits]

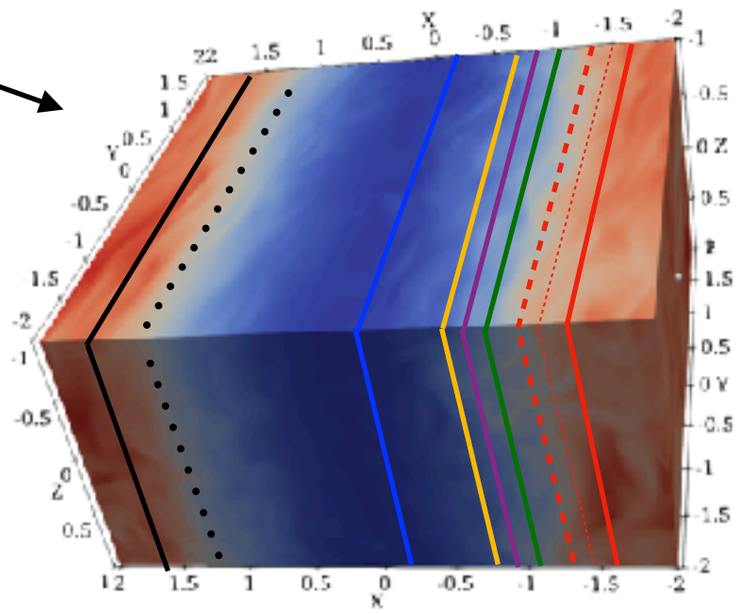

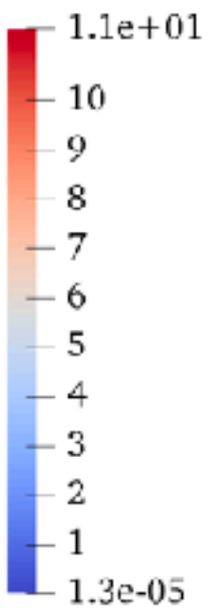

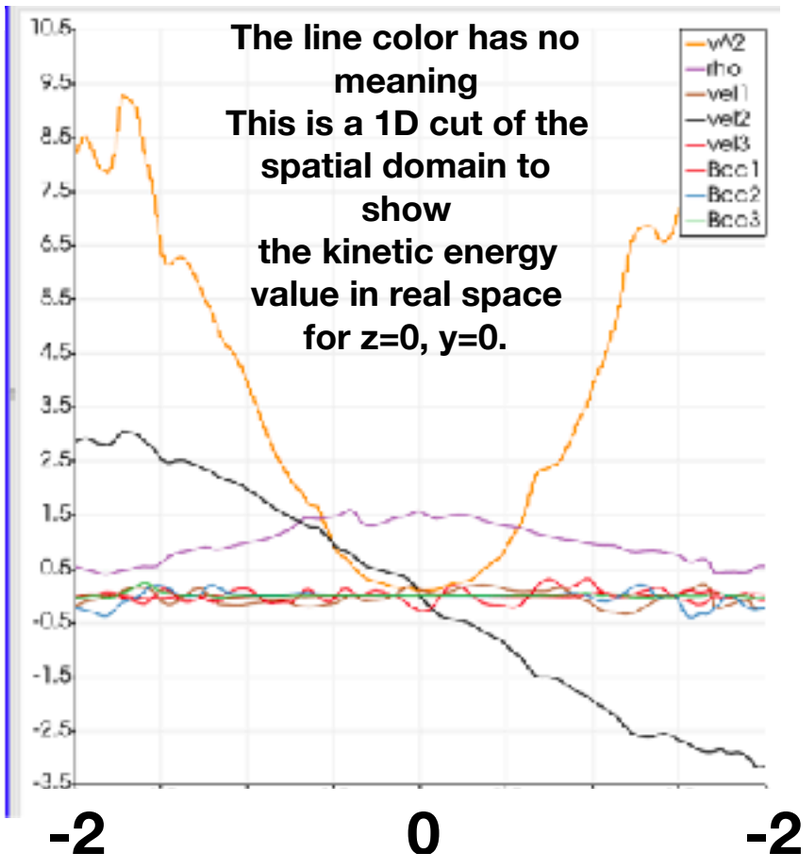

x (radius, in unit of thickness of the disk)

Averaged between t=38.20 [orbits] and t=47.75 [orbits]

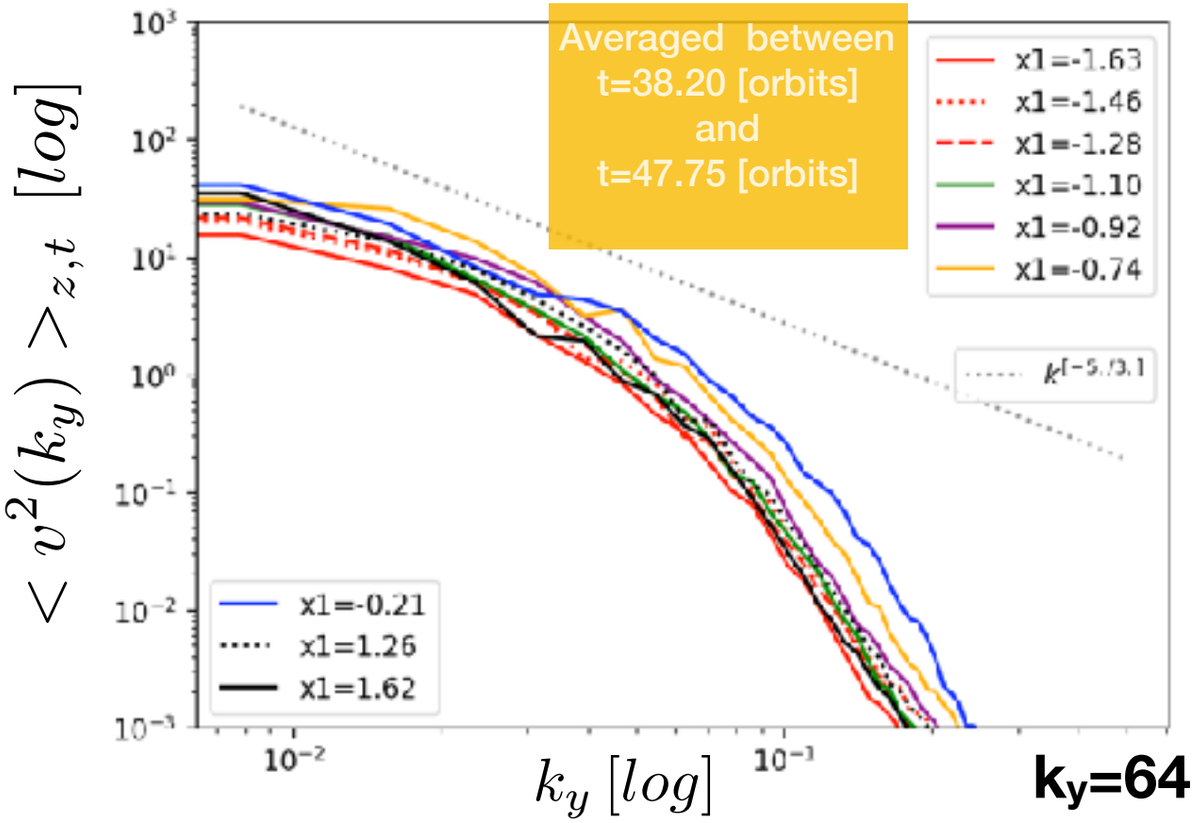

k$_y$=64

!Frequencies are k= 2*pi/L*n
While in the grephs, n is shown

Averaged between t=38.20 [orbits] and t=47.75 [orbits]

Kin 1D spectra: Beta=10^4

$\eta = 10^{-2}$

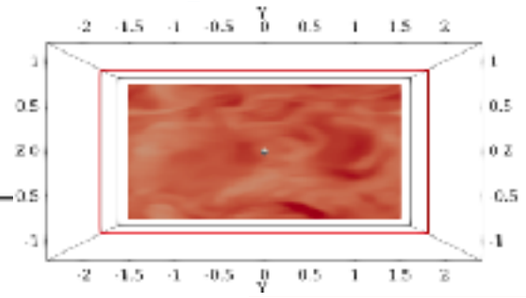

t=38.20 [orbits]

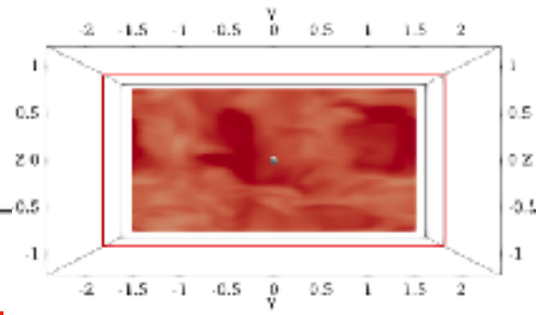

t=47.75 [orbits]

ACTIVE LAYERS

x1=-1.63
x1=-1.46
x1=-1.28
x1=1.26
x1=1.62

$k^{[-5./3.]}$

t=38.20 [orbits]

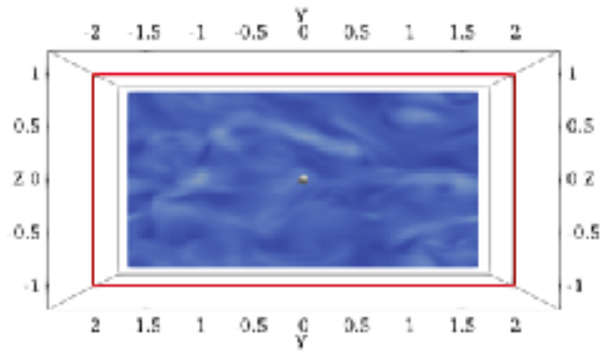

t=47.75 [orbits]

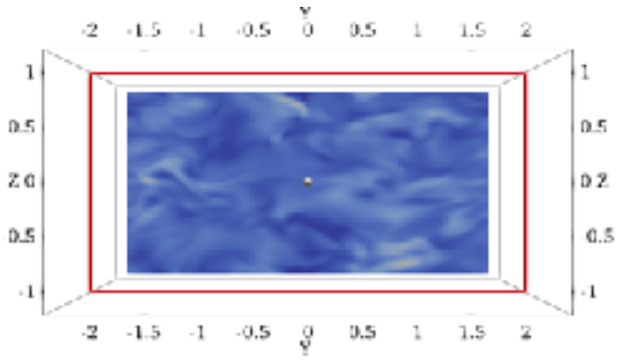

$\delta v_x = v_x$

$\delta v_y = v_y - v_{0y}$

$\delta v_z = v_z$

x1=-1.10
x1=-0.92
x1=-0.74
x1=-0.21

DEAD LAYERS

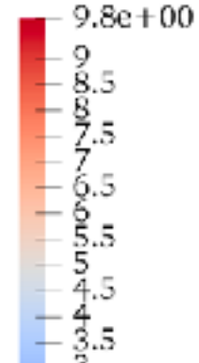

v²

$< |v(k_y, x = x1)|^2 >_{z,t}[log_{10}]$

$k_y[log_{10}]$

Averaged between t=38.20 [orbits] and t=47.75 [orbits]

Mag 1D spectra: Beta=10^4 $\eta = 10^{-2}$

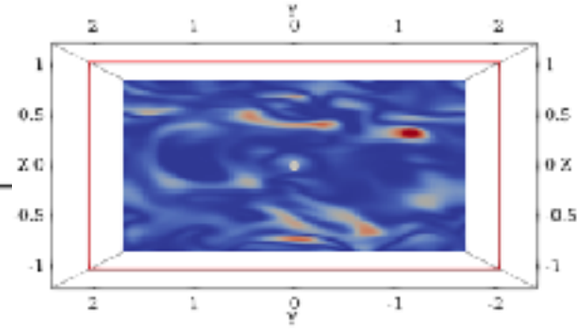

t=38.20 [orbits]

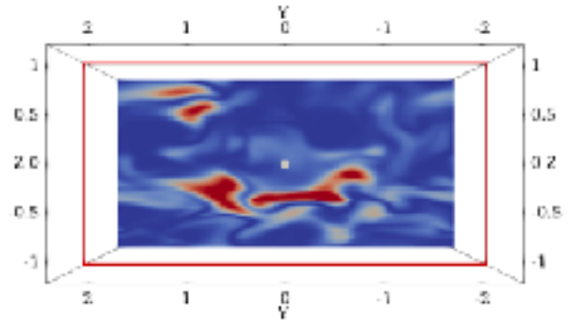

t=47.75 [orbits]

ACTIVE LAYERS

- x1=-1.63
- x1=-1.46
- x1=-1.28
- x1=1.26
- x1=1.62

$k_y^{[-5./3.]}$

DEAD LAYERS

- x1=-1.10
- x1=-0.92
- x1=-0.74
- x1=-0.21

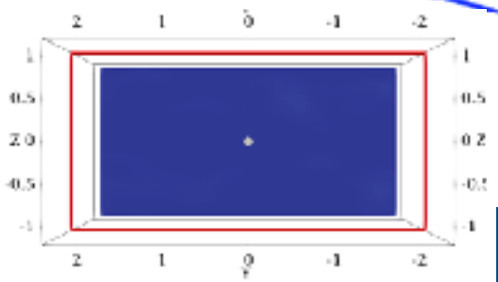

t=47.75 [orbits] Same as t=38.20 [orbits]

2.5e-01, 0.22, 0.2, 0.18, 0.16, 0.14, 0.12, 0.1, 0.08, 0.06, 0.04, 0.02, 0.0e+00 — |B| ^2

$< |B(k_y, x = x1)|^2 >_{z,t} [log_{10}]$

10^1, 10^0, 10^{-1}, 10^{-2}, 10^{-3}

10^0 10^1

$k_y [log_{10}]$

Setup1: 2D Spectra

$$\mathbf{B}(r=\bar{R},\phi,z,t=\bar{t})$$

$$FFT2(\mathbf{B}(r=\bar{R},\phi,z,t=\bar{t})) = \mathcal{F}_\phi\{\mathcal{F}_z\{\mathbf{B}(r=\bar{R},\phi,z,t=\bar{t})\}\}$$

$$:= \tilde{\mathbf{B}}(r=\bar{R},k_\phi,k_z,t=\bar{t})$$

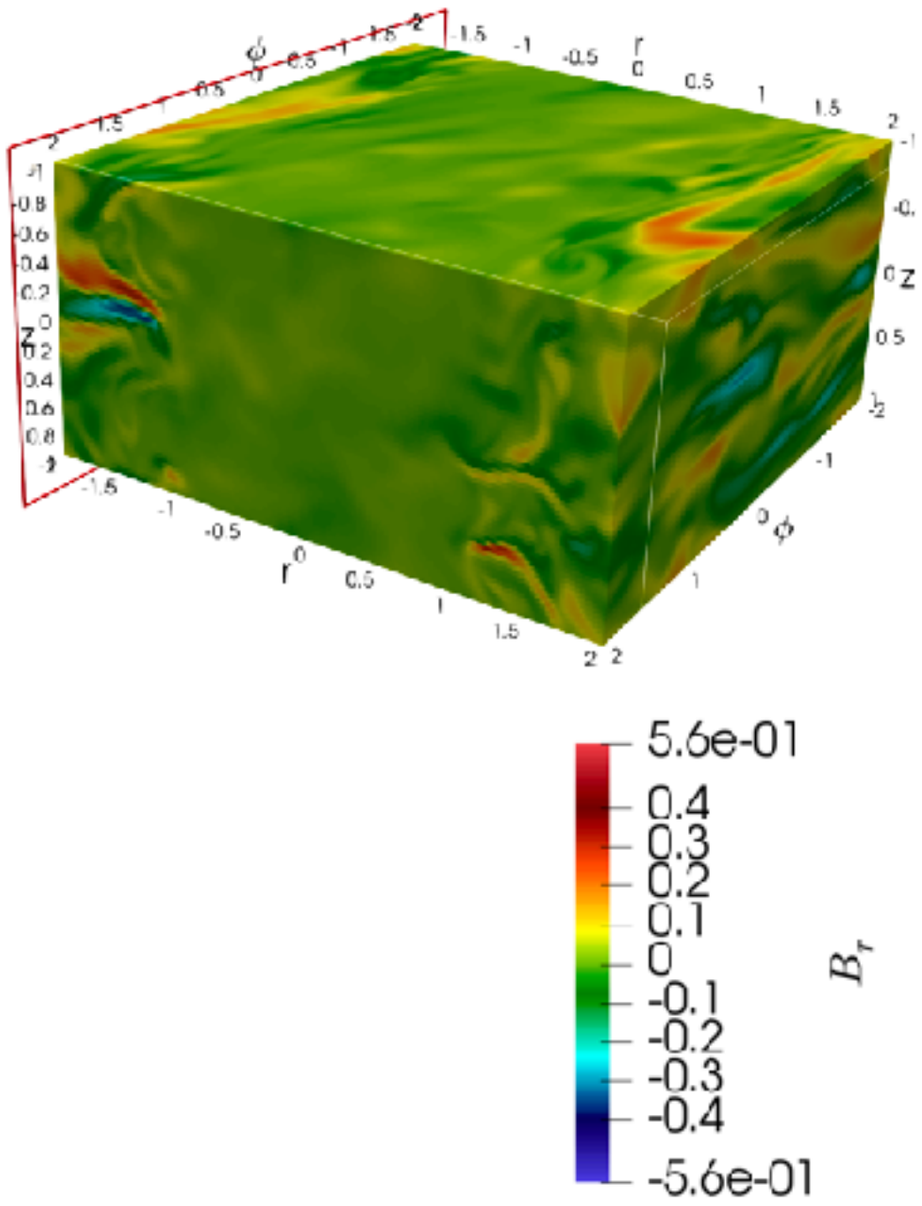

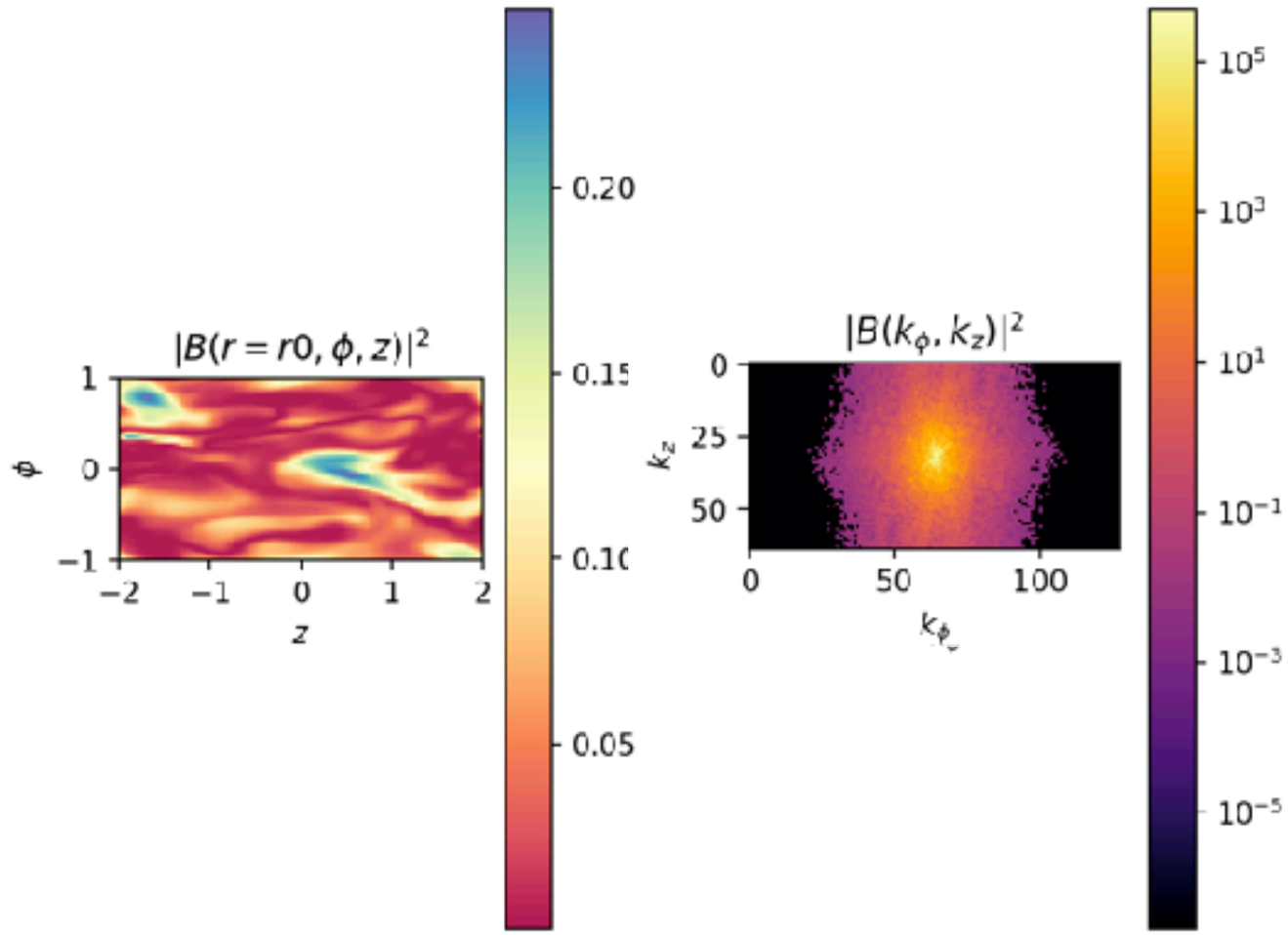

Conclusions

- Develop the diagnostics for the resistive setup: spectra and stress tensors.
- Is the dead zone affected by wave injection from the turbulent zone?
- How do the dead zone boundaries evolve?
- How MRI saturation is affected?

Future work

- Simulate a resistivity which depends on the temperature.
- Relax the isothermal conditions to study the thermodynamics of the disk (see Faure et al. 2014)